

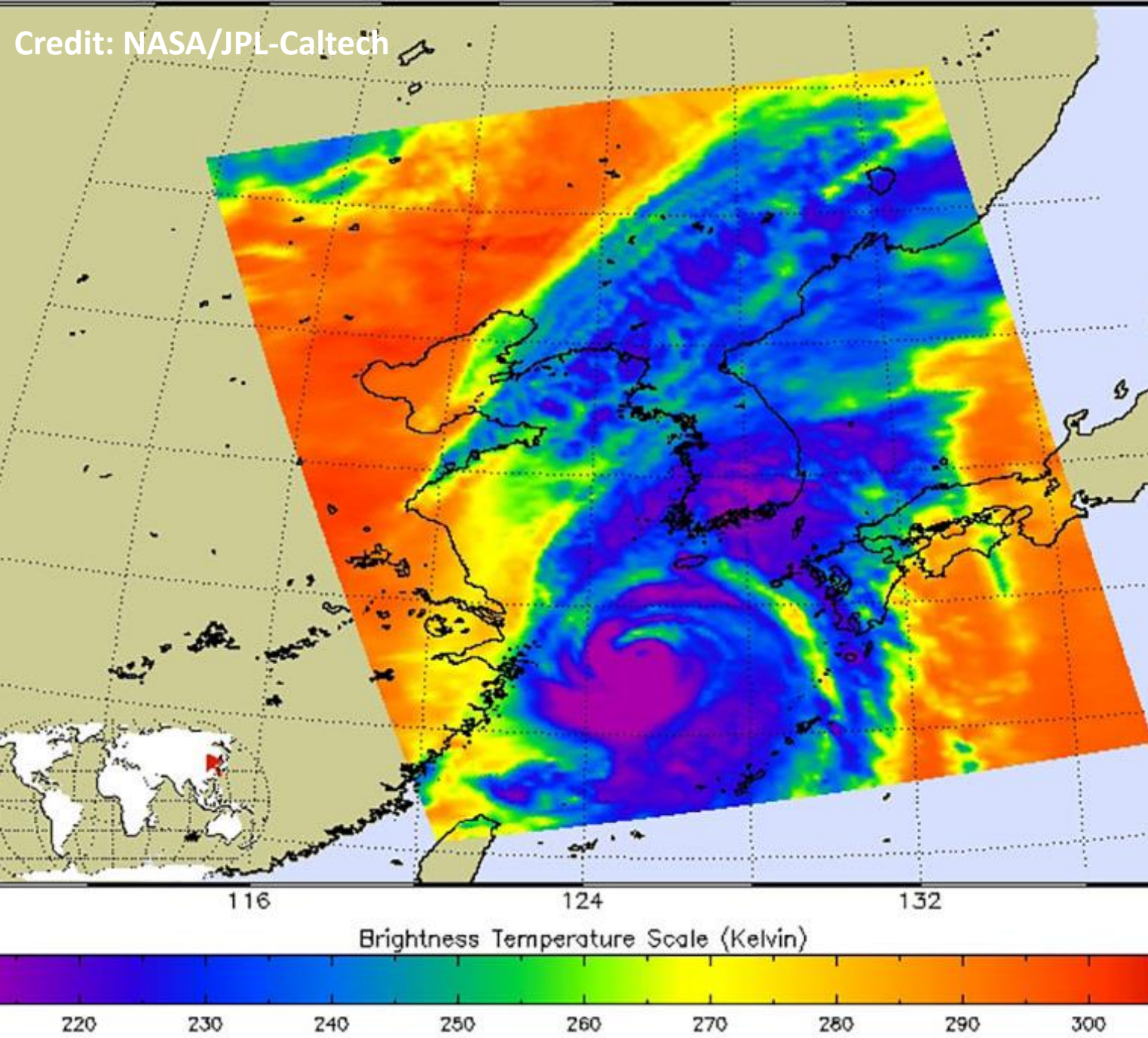
108

116

124

132

Credit: NASA/JPL-Caltech



GPHS-426

Climatology and *Remote Sensing*

RS Lecture 3

11 January 2024

Remote Sensing (4 X 2-hour classes)

Lecturer: Yizhe Zhan

- Principles of satellite remote sensing (Wed 13 Dec 2023)
- Meteorological satellites (Tues 19 Dec 2023)
- **Passive remote sensing instruments (Thurs 11 Jan 2024)**
- Active remote sensing instruments (Thurs 18 Jan 2024)

For course material and hands-on session,



https://github.com/yizhe-met/GPHS-426_RS.git

For reach out for questions, my EDU email is yizhe@illinois.edu.

Outline

1. Continue Course 2 - *Instrument calibration and impact*
2. Overview of remote sensing instruments
3. Passive sensing instruments and products

Broadband Earth radiation radiometer

- Example instrument: CERES
- Example product: TOA-albedo

Moderate resolution optical imager

- Example instrument: MODIS
- Example product: AOD

Moderate resolution optical imager

- Example instrument: AHI
- Example product: CTH

Cross-nadir infrared sounder

- Example instrument: AIRS
- Example product: Temperature profile

Cross-track microwave radiometer

- Example instrument: SSM/I
- Example product: Precipitation

Instrument calibration and impact

Instrument calibration is essential to achieve its mission objectives. In general, it can be divided into the following two categories.

Pre-launch calibration

The key objectives of pre-launch calibration include, but not limited to

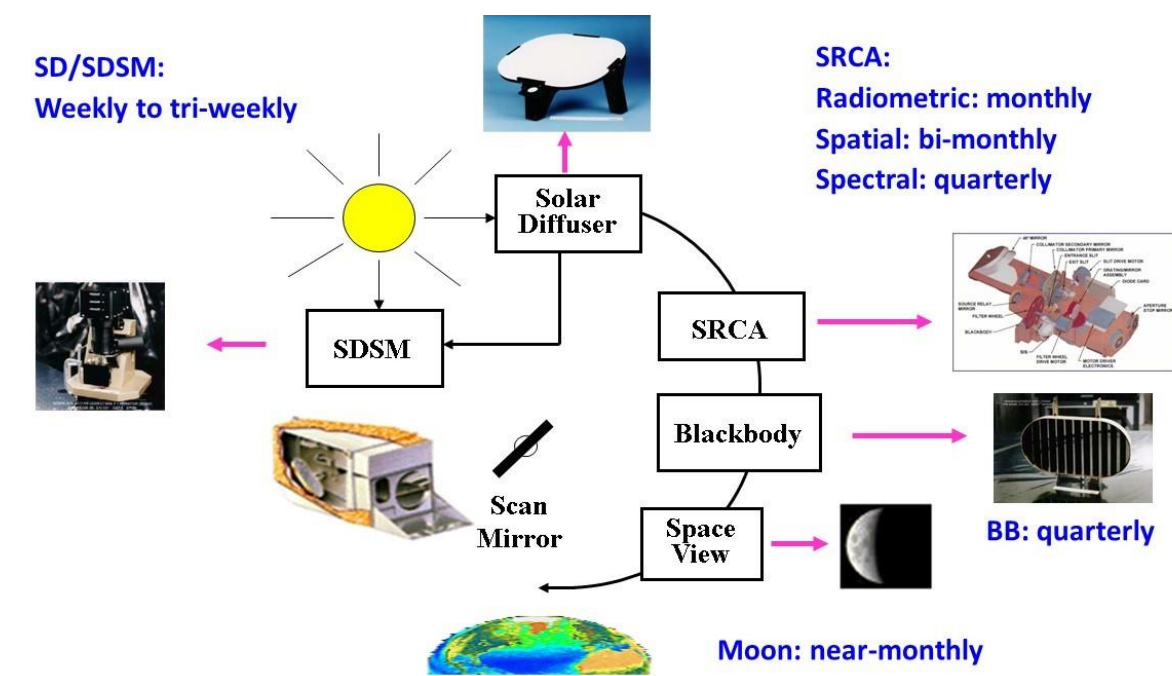
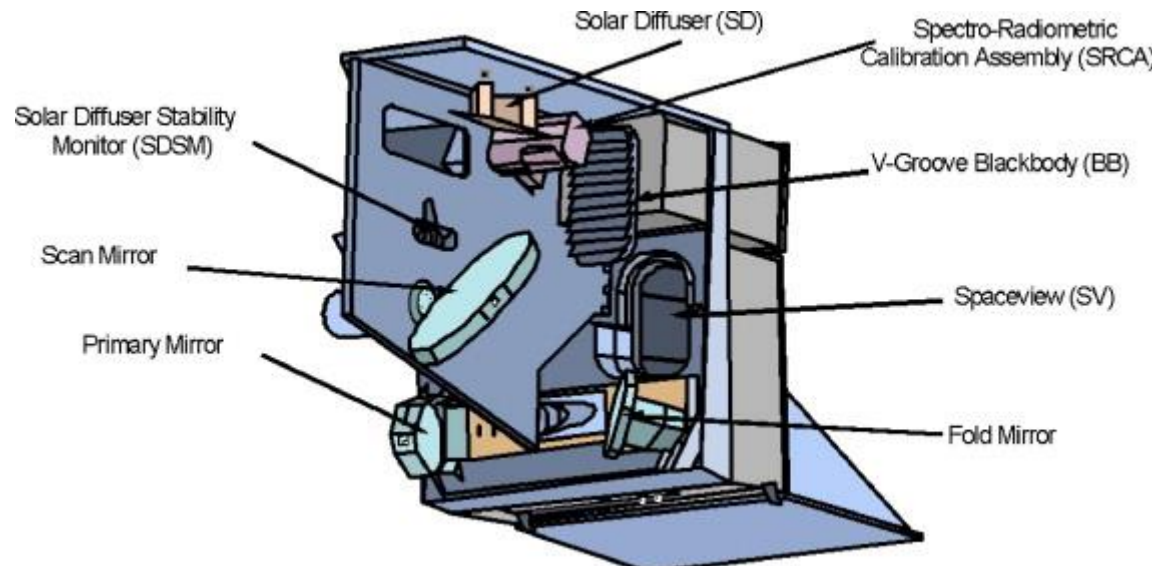
- (1) Evaluating sensor performance under different operating conditions that might be experienced in space;
- (2) Deriving calibration parameters that are needed to support sensor on-orbit calibration and its L1B calibration algorithm;
- (3) Establishing sensor calibration traceability and accuracy with reference measurements and comprehensive data analyses to help identify and quantify all contributors to the end-to-end calibration error budget.

On-orbit calibration (Onboard calibration)

The key objectives of onboard calibration include, but not limited to

- (1) Ensuring data accuracy and maintain data consistency;
- (2) Validating instrument performance against pre-launch specifications and detect any degradation and shifts;
- (3) Identifying any gradual changes or 'drift' in instrument behavior and apply corrections to the collected data, ensuring that it remains reliable throughout the mission's duration;
- (4) Providing a basis for comparing and harmonizing data from different instruments across multiple satellites or with ground-based observation systems.
- (5) Enabling the integration of data from multiple sources by ensuring that each dataset is calibrated to a common standard.

Instrument calibration and impact – example



Four OBCs on MODIS:

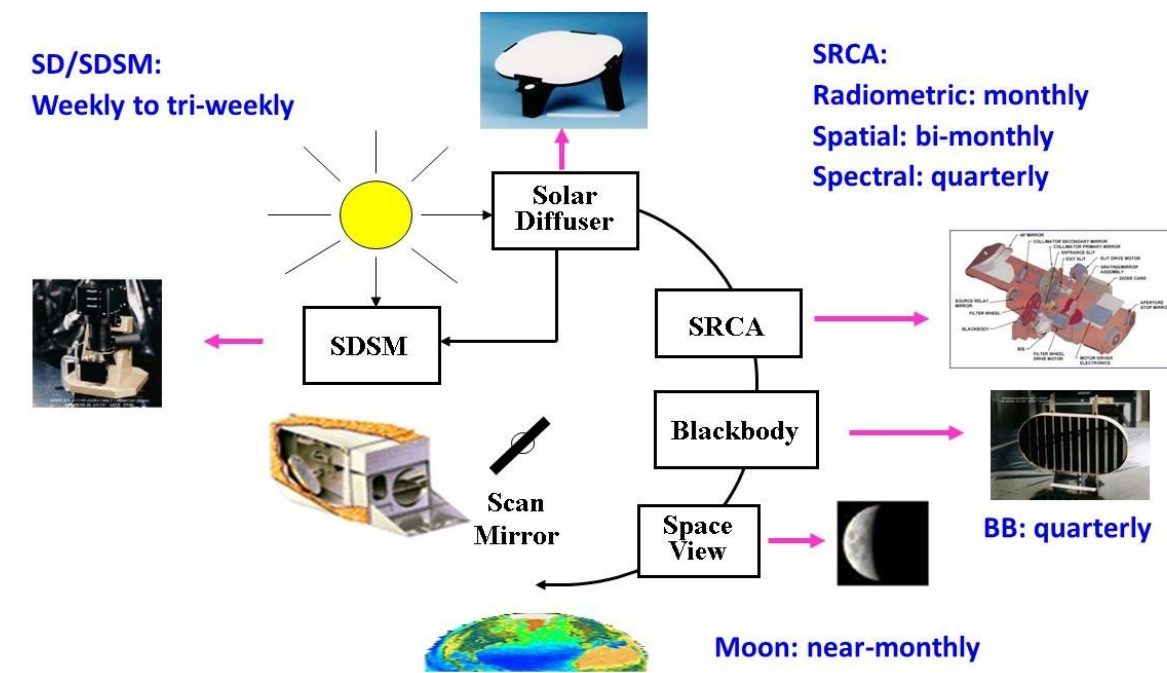
- BB – Blackbody -> mid- and long-wave infrared bands ($3.5 \mu\text{m} \sim 14.4 \mu\text{m}$)
- SD – Solar Diffuser -> visible, near infrared bands ($0.4 \mu\text{m} \sim 2.2 \mu\text{m}$)
- SDSM – Solar Diffuser Stability Monitor
- SRCA – Spectroradiometric Calibration Assembly

Schematic of MODIS on-orbit calibration and characterization approaches and nominal scheduling frequencies.

Xiong and Butler (2020)

Instrument calibration and impact – example

- The degradation of the MODIS response is wavelength, mirror-side, and angle-of-incidence (AOI) dependent [Guenther et al., 2002; Xiong et al., 2002], and thought to be caused by thin film depositions on optics followed by solarization of that film through ultraviolet exposure [Guenther et al., 2002].
- The degradation of the MODIS SD, however, is wavelength dependent [Xiong et al., 2002].
- Based on the first year of MODIS data, Guenther et al. [2002] showed there were 0.2% and 0.5% SD degradation for MODIS bands 1 and 2, respectively.
- These degradations increased to 0.8% and 0.5% after nearly 2.5 years [Xiong et al., 2002].
- Recent studies of several Terra visible (VIS) and NIR bands show, however, a systematic wavelength-dependent drift of 2%–6% since 2003, and Terra-MODIS bands 1 and 2 suffered a drift of ~2% [Wu et al., 2013].
- These all indicated the inadequacies in the MODIS SD/SDSM calibration system [Wu et al., 2013].



Schematic of MODIS on-orbit calibration and characterization approaches and nominal scheduling frequencies.

Xiong and Butler (2020)

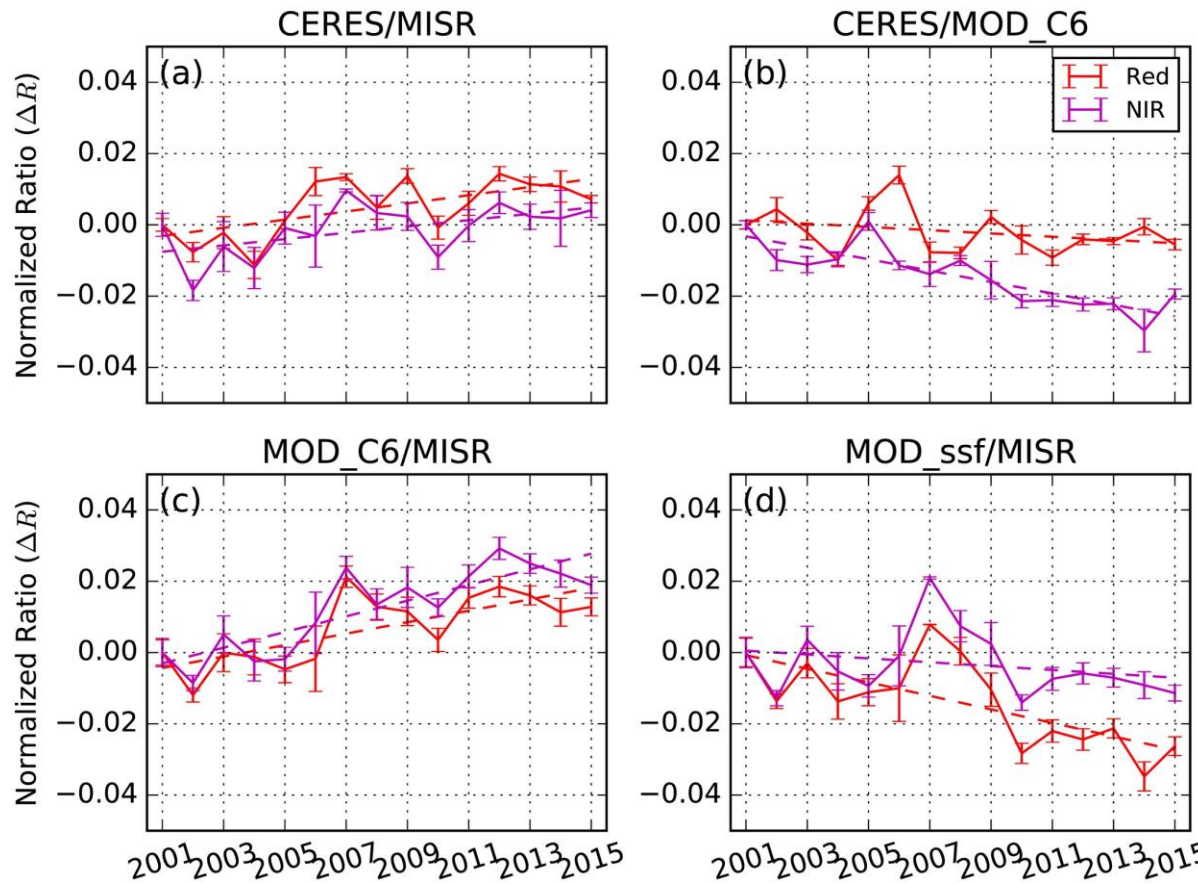
Instrument calibration and impact – example

Summary of Terra MODIS L1B data collections and key calibration updates.

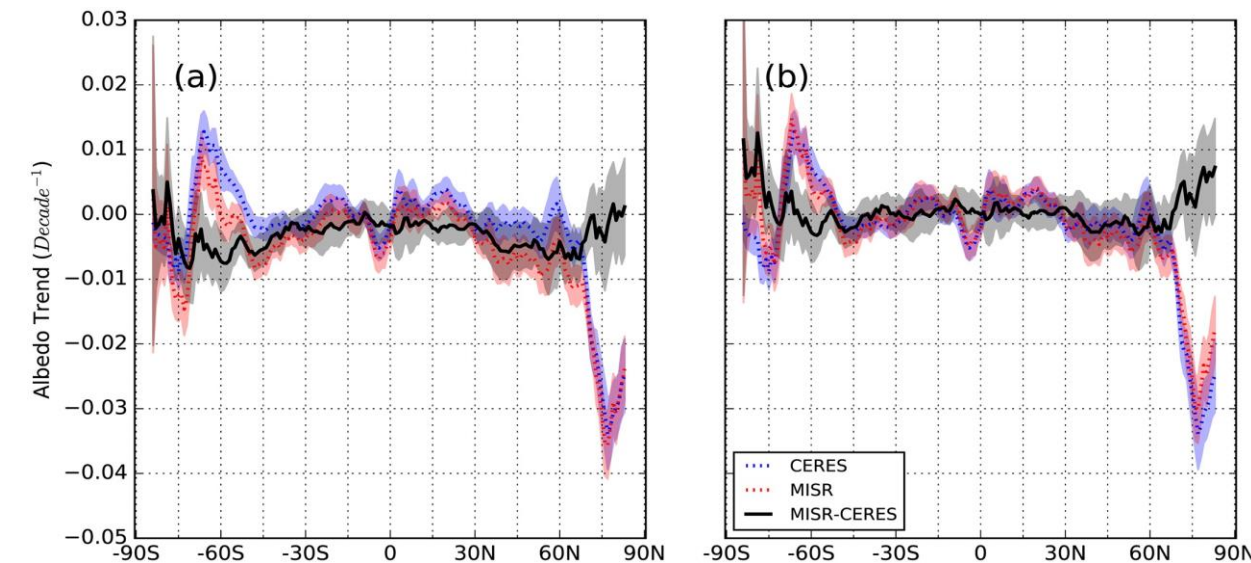
MODIS Collection	Time range	Improvements
Collection 2	03/2000–05/2001	Improvement of SWIR Crosstalk Correction Algorithm; <DN_SV> Computation When Moon is in SV Port for TEB.
Collection 3	05/2001–01/2003	Piecewise linear time dependent LUT implemented; <DN_SV> computation when Moon is in SV port for RSB.
Collection 4	01/2003–04/2007	Band 26 correction using band 5; time dependent RVS for bands 3, 8, and 9 using SD, lunar and SRCA gains.
Collection 5	03/2005–03/2017	Detector-dependent SWIR cross-talk correction, mirror-side dependent band 21 calibration; pitch maneuver derived RVS for TEB; time-dependent RSB RVS was extended to bands 1-4, 8-12, 17-19, using SD, lunar, and EV mirror-side ratios; mirror side 2 RSB RVS are normalized to mirror side 1.
Collection 6	11/2012–present	RSB RVS changed to quartic from quadratic; improved uncertainty algorithm for both RSB and TEB; TEB a0/a2 LUTs derived from BB cool-down data; EV-based RVS for bands 1-4, 8-10; correction for SD degradation at 936 nm (SDSM D9) and beyond; detector dependent RVS for bands 3, 8-12; SWIR sending band switched from 28 to 25.
Collection 6.1	09/2017–present	Crosstalk correction algorithm applied to LWIR PV bands (27-30); QA LUT updated due to changes made; SWIR sending band switched from 28 to 25.

Xiong and Butler (2020)

Instrument calibration and impact – example



Greenland Spot case of normalized radiance ratio trends for successive Aprils, for (a) CERES against MISR, (b) CERES against MODIS Collection 6, (c) MODIS Collection 6 against MISR, and (d) MODIS SSF against MISR. Data were limited to $0.07 \leq \text{PWC} \leq 0.12 \text{ cm}$.



Latitudinal decadal trend of TOA albedo, (a) before and (b) after applying a correction coefficient of +1% decade $^{-1}$ for CERES-MISR intercalibration.

Forward and inverse problems

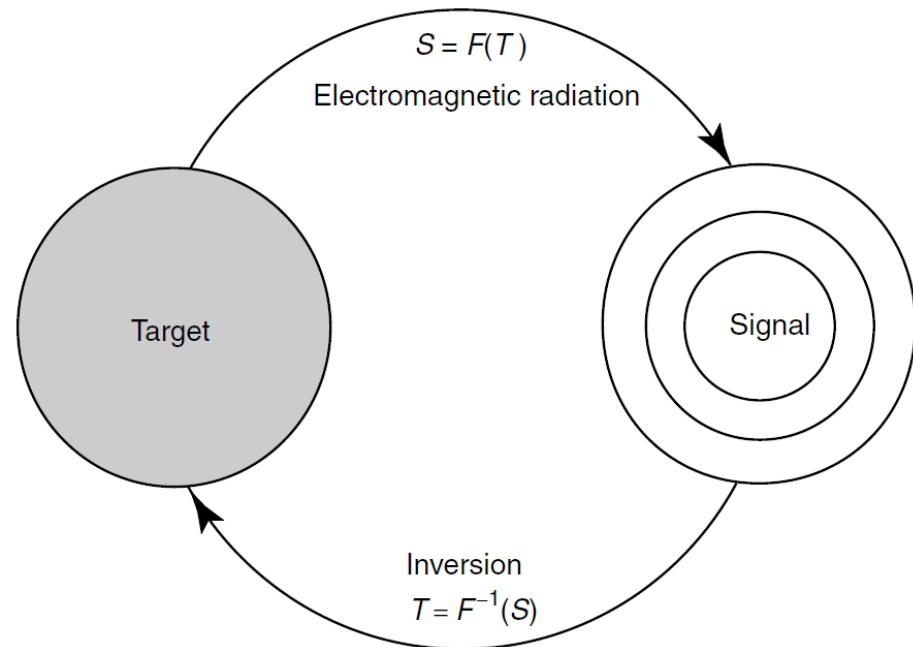


Figure 7.1 Principle of remote sensing. The symbols T and S denote target and signal, respectively, F represents a function which is generally nonlinear and cannot be represented by analytic equations, and F^{-1} is the inverse of this complicated function.

In remote sensing, the concepts of forward and inverse problems are fundamental to understanding how remote sensing data is processed and interpreted.

These concepts are central to the retrieval of meaningful information about the Earth's surface and atmosphere from the data collected by remote sensing instruments.

Forward Problems: Predicting what a sensor will observe, based on known ground conditions.

e.g., predicting the radiance values that a satellite sensor should record for a specific type of vegetation cover under known illumination and atmospheric conditions.

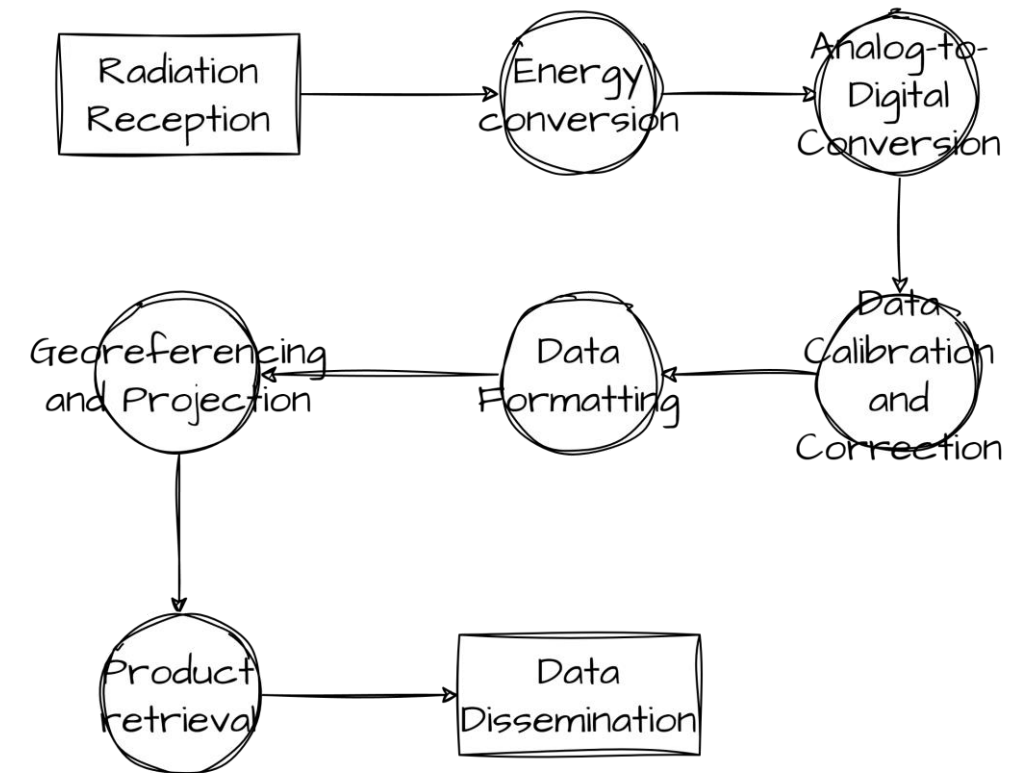
Inverse Problems: Determining ground conditions or properties from observed sensor data.

e.g., determining the type of vegetation and its health from the spectral radiance values recorded by a satellite sensor.

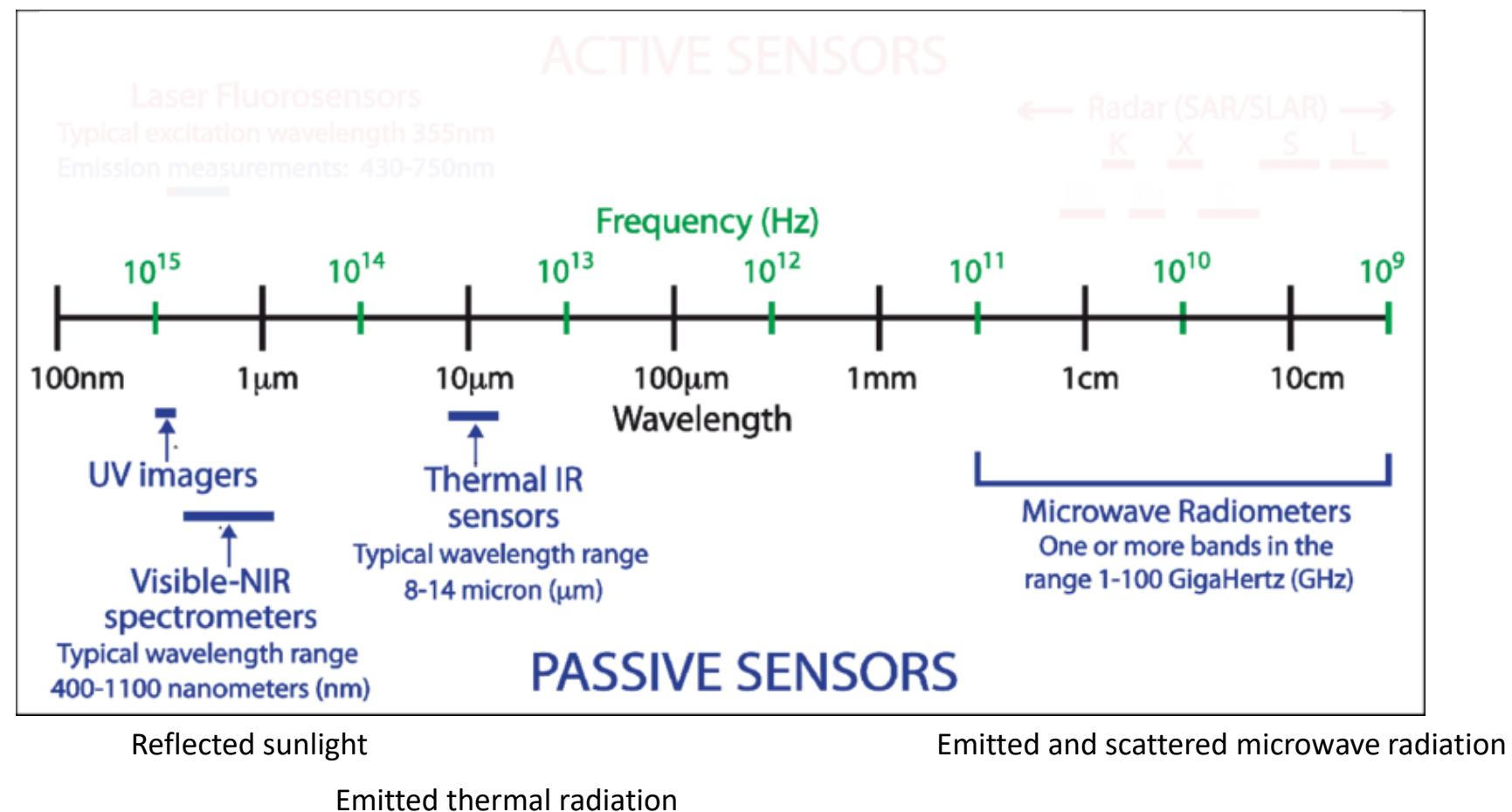
Overall workflow

Passive sensing systems in satellite remote sensing convert the received electromagnetic radiation into digital data through a series of steps:

1. **Radiation reception:** detect electromagnetic radiation naturally emitted or reflected by the Earth's surface and atmosphere.
2. **Energy conversion:** convert the incoming radiation into an electrical signal.
3. **ADC:** convert the analog electrical signal to digital format.
4. **Calibration and correction:** calibrate and correct raw digital data for sensor noise, drift, etc.
5. **Data formatting:** format the calibrated digital data into usable form (e.g., image, data array).
6. **Georeferencing and projection:** assign each pixel a specific geographic location on the Earth's surface.
7. **Product retrieval:** produce specific products using operational retrieval algorithms.
8. **Data dissemination:** make the processed digital data available to users.

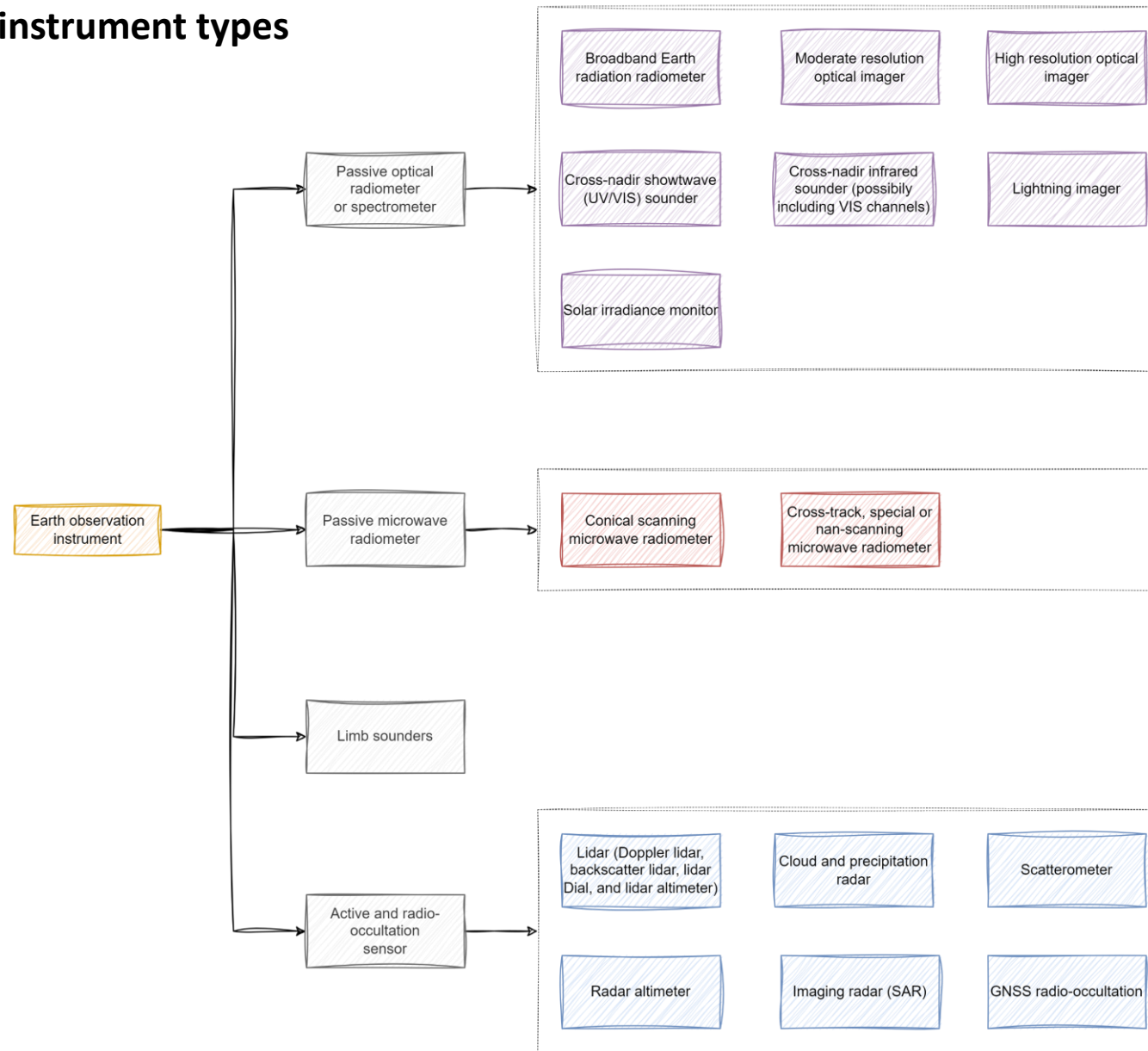


Remote sensing instruments (sensors)



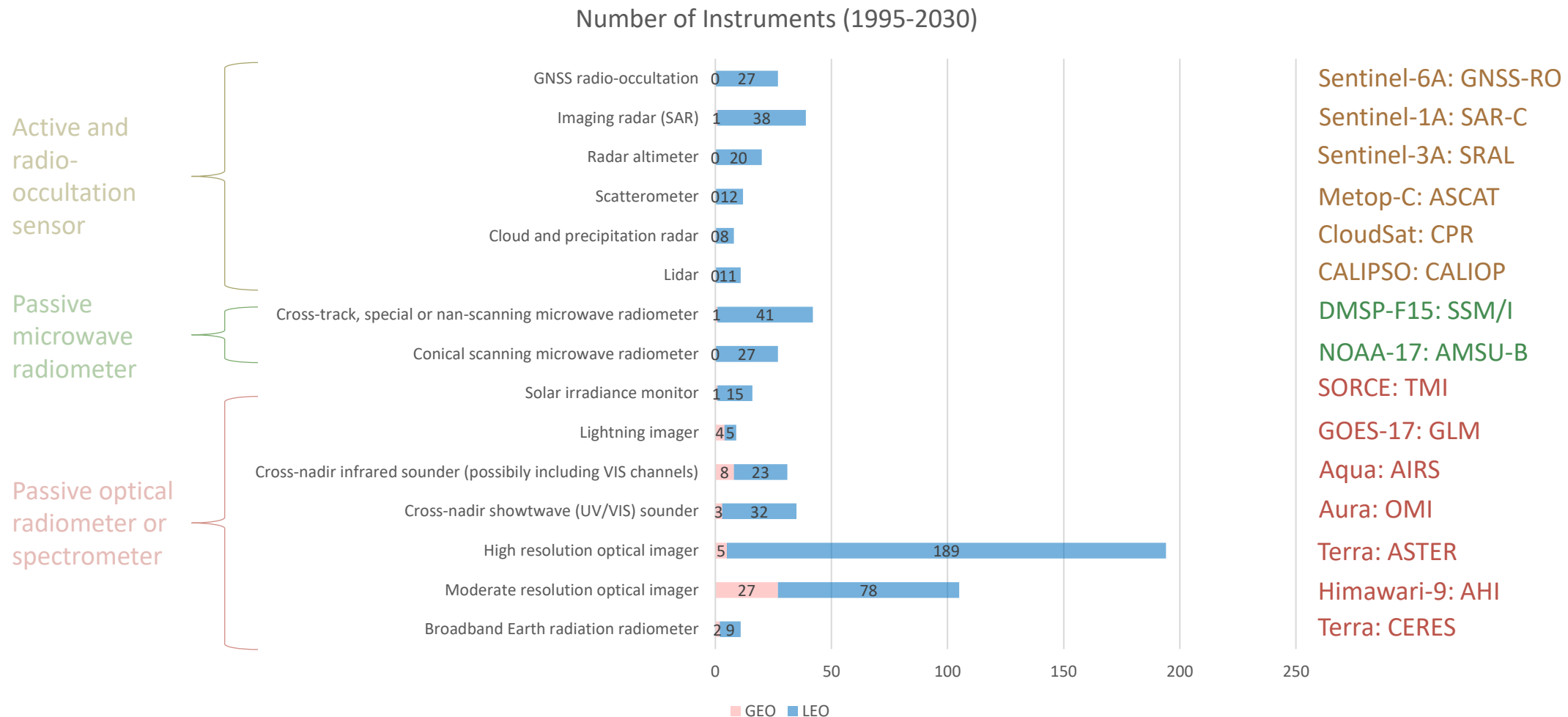
$$T_\lambda + A_\lambda + R_\lambda = 1$$

Earth observation instrument types



Data source: OSCAR

Earth observation instrument types (with examples)



Data source: OSCAR

NASA Terra Satellite: ACCESS to Terra Data Fusion Products



Data Fusion Visualization for NASA CAMP2Ex Field Campaign



Broadband Earth radiation radiometer

- Example instrument: CERES
- Example product: TOA-albedo

Moderate resolution optical imager

- Example instrument: AHI
- Example product: CTH

Cross-track microwave radiometer

- Example instrument: SSM/I
- Example product: Precipitation

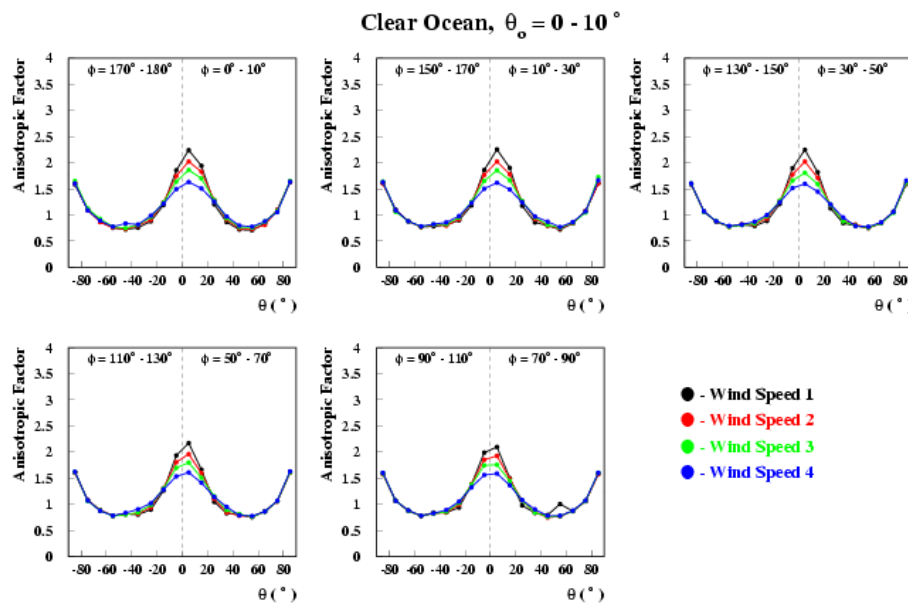
Moderate resolution optical imager

- Example instrument: MODIS
- Example product: AOD

Cross-nadir infrared sounder

- Example instrument: AIRS
- Example product: Temperature profile

TOA albedo (SW flux) retrieval



CERES/TRMM SSF Edition2B ADMs for
clear-sky ocean ($\theta_0 = 0 \sim 10^\circ$)

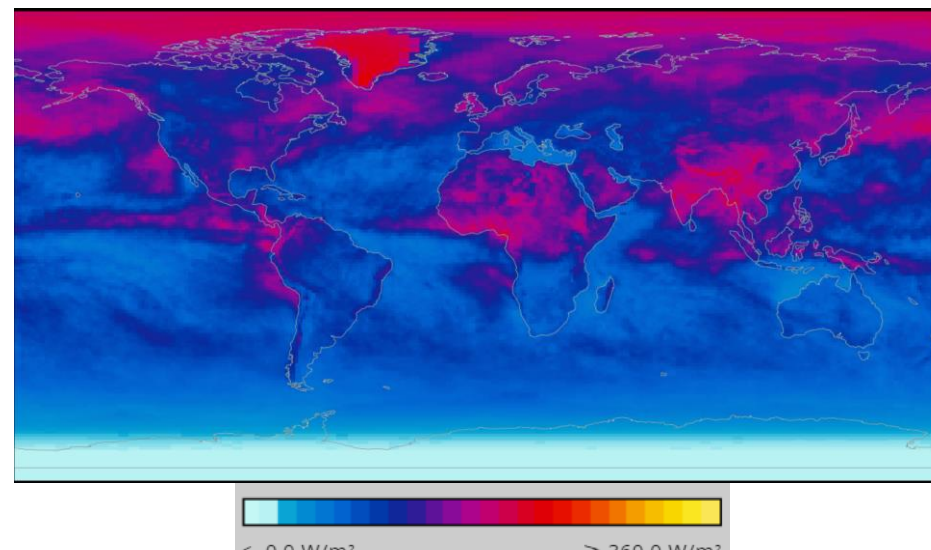
Retrieving TOA-albedo is equivalent to TOA radiative flux retrieval over shortwave broadband.
From Course 1, we know that

$$F_\lambda = \int_{\Omega} I_\lambda \cos\theta d\Omega = \int_0^{2\pi} \int_0^{\pi/2} I_\lambda(\theta, \phi) \cos\theta \sin\theta d\theta d\phi$$

However, satellite cannot *view* all angles simultaneously. And scenes are not Lambertian. As a result, the main idea of TOA flux retrieval is to have a pre-calculated set of anisotropic factor, $R_j(\theta_0, \theta, \phi)$, so that

$$F_{SW}(\theta_0) = \frac{\pi I_{SW}(\theta_0, \theta, \phi)}{R_j(\theta_0, \theta, \phi)}$$

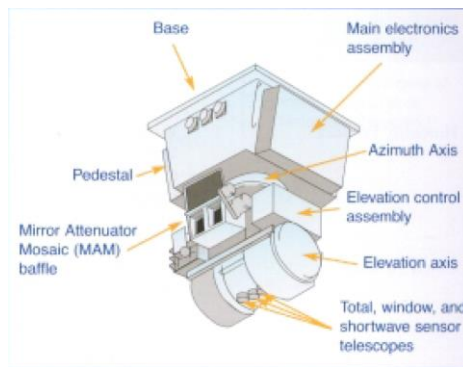
For shortwave spectrum, the scene anisotropic characteristics is impacted by surface, cloud, aerosol properties. To account for different anisotropic scenes, the most convenient way is to build a set of ADMs (Angular Distribution Models) to account for each distinct scene type.



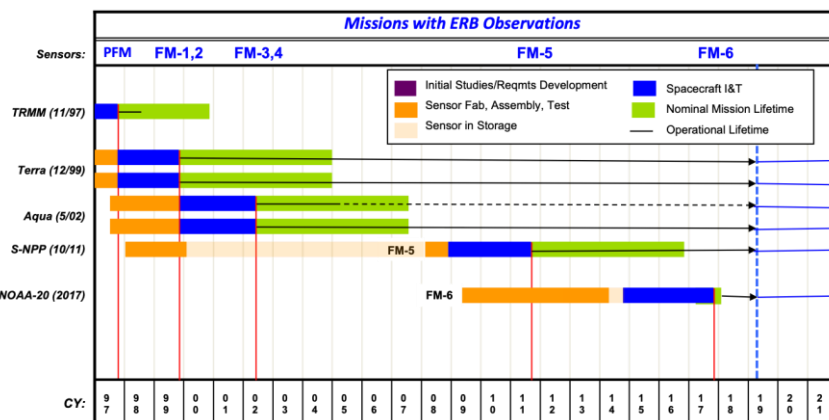
Su et al., (2015)

Broadband Earth radiation radiometer

- Example instrument: CERES
- Example product: TOA-albedo



CERES Flight Schedules



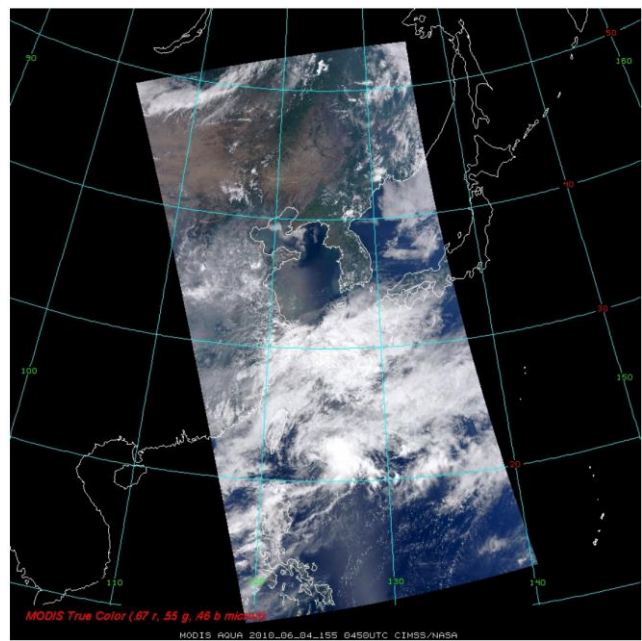
The goals of the CERES project are to:

1. Produce a long-term, integrated global climate data record for detecting decadal changes in the Earth's radiation budget from the surface to the top-of-atmosphere.
2. Enable improved understanding of how Earth's radiation budget varies in time and space and the role that clouds and other atmospheric properties play.
3. Support climate model evaluation and improvement through model-observation intercomparisons.

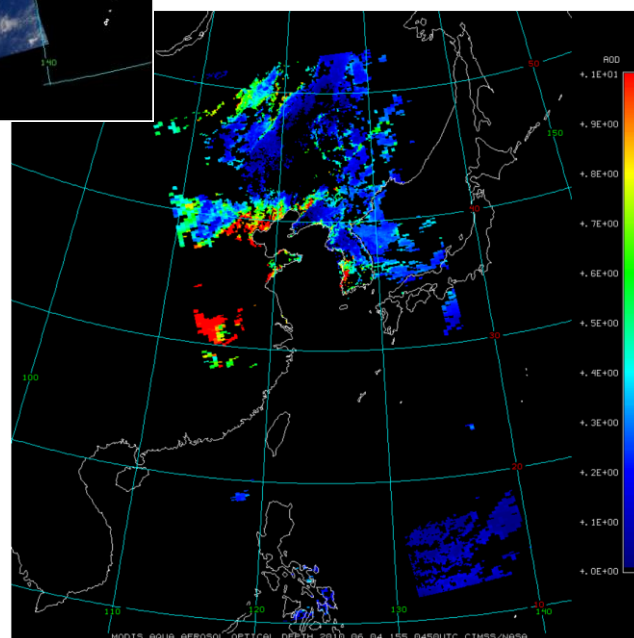
Seven CERES instruments on five satellites have been launched (TRMM, Terra, Aqua, S-NPP, NOAA-20). Six of the seven are currently operational.

- Each CERES instrument is a narrow field-of-view scanning radiometer with nadir footprint size of 10 km (TRMM), 20 km (Terra, Aqua), or 24 km (S-NPP, NOAA-20).
- CERES instruments measure broadband radiances in 0.3-5 μm (SW), 0.3-200 μm (TOT) and 8-12 μm (WN) channels. On NOAA-20, the FM6 instrument replaces the WN channel with a LW channel (5-35 μm).
- Each CERES instrument can scan in three principal modes: fixed azimuth plane (FAP) or crosstrack, rotating azimuth plane (RAP), and programmable azimuth plane (PAP).
- Onboard calibration sources include a solar diffuser, a tungsten lamp system with a stability monitor, and a pair of blackbodies that can be controlled at different temperatures. Cold space looks and internal calibration are performed during nominal Earth scans. The CERES instruments also periodically scan the moon, which is used as an additional check on instrument radiometric stability.

Aerosol Optical Depth retrieval



Example of MODIS AOD product on 2010-06-04 at 0450 UTC



Atmospheric aerosols play a crucial role in Earth's energy budget by scattering and absorbing radiation, which contributes to the global climate system, and they also contribute to cloud formation and precipitation by acting as condensation nuclei for clouds (Trenberth et al., 2009).

AOD (Aerosol Optical Depth) is a measure of the vertically integrated extinction (scattering and absorption) of solar radiation by atmospheric aerosol particles.

The Moderate Resolution Imaging Spectroradiometer (MODIS) sensor on board the Terra and Aqua satellites is one of the oldest operational instruments and has provided atmospheric observations for almost two decades.

MODIS has two well-known aerosol retrieval algorithms: Dark Target (DT) and Deep Blue (DB) (Hsu et al., 2013; Levy et al., 2013). The DT retrieval algorithm provides aerosol data over dark pixels, such as vegetation and ocean areas.

The Dark Target (DT) algorithm essentially follows the Single-scattering approximation we showed in Course 1 (Eq. 7),

$$R_\lambda(\mu, \phi; \mu_0, \phi_0) = \frac{\pi I_\lambda(0; \mu, \phi)}{\mu_0 F_\odot} = \tau_* \frac{\tilde{\omega}}{4\mu\mu_0} P(\mu, \phi; -\mu_0, \phi_0)$$

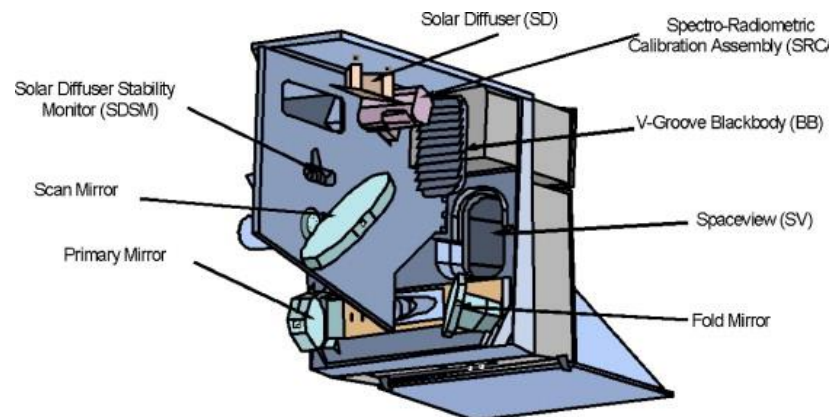
The AOD (τ_*) can be calculated using

$$\tau_* = \frac{R_\lambda(\mu, \phi; \mu_0, \phi_0)}{P(\mu, \phi; -\mu_0, \phi_0)} \frac{4\mu\mu_0}{\tilde{\omega}}$$

where $P(\mu, \phi; -\mu_0, \phi_0)$ and $\tilde{\omega}$ are aerosol phase function and single scattering albedo, respectively. Because the aerosol size distribution and the refractive indices are generally unknown *a priori*, $P(\mu, \phi; -\mu_0, \phi_0)$ and $\tilde{\omega}$ must be assumed or parameterized from other information. In this manner, a measured R_λ will yield an optical depth for the atmosphere. In practice, the relationship between scene type and P , $\tilde{\omega}$ were pre-calculated and stored as LUT.

Moderate resolution optical imager

- Example instrument: MODIS
- Example product: AOD



What is MODIS:

1. Moderate-Resolution Imaging Spetroradiometer
2. Launched in 1999 aboard the EOS AM (Terra); EOS PM (Aqua) followed in 2002
3. Monitors 36 spectral bands between 0.4 μm and 14.4 μm
4. Images entire Earth every 1-2 days at 0.25 – 1 km resolution
5. MODIS data are used for a wide variety of Atmosphere, Land, and Ocean applications.

Primary Use	Band	Bandwidth ¹	Spectral Radiance ²	Required SNR ³	Spatial Resolution
Land/Cloud/Aerosols Boundaries	1	620 - 670	21.8	128	250 meters
	2	841 - 876	24.7	201	
Land/Cloud/Aerosols Properties	3	459 - 479	35.3	243	500 meters
	4	545 - 565	29.0	228	
Ocean Color/Phytoplankton/Biogeochemistry	5	1230 - 1250	5.4	74	500 meters
	6	1628 - 1652	7.3	275	
Atmospheric Water Vapor	7	2105 - 2155	1.0	110	1000 meters
	8	405 - 420	44.9	880	
Cirrus Clouds	9	438 - 448	41.9	838	1000 meters
	10	483 - 493	32.1	802	
Atmospheric Water Vapor	11	526 - 536	27.9	754	1000 meters
	12	546 - 556	21.0	750	
Cirrus Clouds	13	662 - 672	9.5	910	1000 meters
	14	673 - 683	8.7	1087	
Atmospheric Water Vapor	15	743 - 753	10.2	586	1000 meters
	16	862 - 877	6.2	516	
Atmospheric Water Vapor	17	890 - 920	10.0	167	1000 meters
	18	931 - 941	3.6	57	
Cirrus Clouds	19	915 - 965	15.0	250	1000 meters
	26	1380			

Primary Atmospheric Application	Band	Bandwidth ¹	T _{typical} (K)	Radiance ² at T _{typical}	NEAT (K) Specification	NEAT (K) Predicted
Surface Temperature	20	3.660-3.840	300	0.45	0.05	0.05
	22	3.929-3.989	300	0.67	0.07	0.05
	23	4.020-4.080	300	0.79	0.07	0.05
Temperature profile	24	4.433-4.498	250	0.17	0.25	0.15
	25	4.482-4.549	275	0.59	0.25	0.10
Moisture profile	27	6.535-6.895	240	1.16	0.25	0.05
	28	7.175-7.475	250	2.18	0.25	0.05
	29	8.400-8.700	300	9.58	0.05	0.05
Ozone	30	9.580-9.880	250	3.69	0.25	0.05
Surface Temperature	31	10.780-11.280	300	9.55	0.05	0.05
	32	11.770-12.270	300	8.94	0.05	0.05
Temperature profile	33	13.185-13.485	260	4.52	0.25	0.15
	34	13.485-13.785	250	3.76	0.25	0.20
	35	13.785-14.085	240	3.11	0.25	0.25
	36	14.085-14.385	220	2.08	0.35	0.35

Cloud top height retrieval

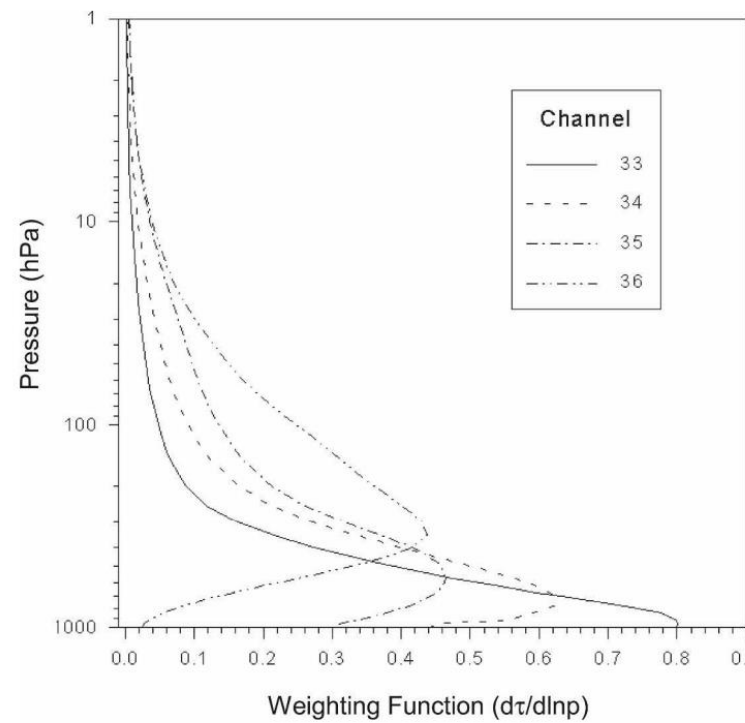


FIG. 1. Weighting functions for the four MODIS bands in the CO₂ absorption band.

Temperature profile	33	13.185-13.485	260	4.52	0.25	0.15
	34	13.485-13.785	250	3.76	0.25	0.20
	35	13.785-14.085	240	3.11	0.25	0.25
	36	14.085-14.385	220	2.08	0.35	0.35

- Consider a FOV consisting of a cloud layer located at a pressure level p_c with a temperature T_c . η is the cloud cover fraction and ε_ν is the cloud emissivity.
- Consider monochromatic radiative transfer such that the transmittance multiplication follows exponential operations.

The radiance observed at the satellite can be written,

$$I_\nu = (1 - \eta \varepsilon_\nu) \left[B_\nu(T_s) T_\nu(p_s, p_c) + \int_{p_s}^{p_c} B_\nu(p) \frac{\partial T_\nu(p, p_c)}{\partial p} dp \right] T_\nu(p_c, 0) \\ + \eta \varepsilon_\nu B_\nu(T_c) T_\nu(p_c, 0) + \int_{p_c}^0 B_\nu(p) \frac{\partial T_\nu(p, 0)}{\partial p} dp$$

where T_ν is the monochromatic transmittance

$$T_\nu(p_1, p_2) = \exp\left(-\frac{1}{g} \int_{p_1}^{p_2} k_\nu(p) q(p) dp\right)$$

For clear-sky, we have $\eta \varepsilon_\nu = 0$,

$$I_\nu^{clr} = B_\nu(T_s) T_\nu(p_s, 0) + \int_{p_s}^0 B_\nu(p) \frac{\partial T_\nu(p, 0)}{\partial p} dp$$

By subtracting clear-sky radiance from the total radiance, we could derive,

$$I_\nu - I_\nu^{clr} = \eta \varepsilon_\nu \int_{p_s}^{p_c} T_\nu(p, 0) \frac{\partial B_\nu(p)}{\partial p} dp$$

Cloud top height retrieval

The cloud-top pressure for a given cloud element can be derived from radiance ratios between two spectral bands following the work of *Smith and Platt (1978)*. The ratio of the deviations in observed radiances $I(\nu)$ to their corresponding clear-sky radiances $I_{clr}(\nu)$ for two spectral bands of wavenumber ν_1 and ν_2 , viewing the same FOV, is written as

$$\frac{I_{\nu_1} - I_{\nu_1}^{clr}}{I_{\nu_2} - I_{\nu_2}^{clr}} = \frac{\eta \varepsilon_{\nu_1} \int_{p_s}^{p_c} T_{\nu_1}(p, 0) \frac{\partial B_{\nu_1}(p)}{\partial p} dp}{\eta \varepsilon_{\nu_2} \int_{p_s}^{p_c} T_{\nu_2}(p, 0) \frac{\partial B_{\nu_2}(p)}{\partial p} dp}$$

For frequencies that are spaced closely in wavenumber, the **assumption** is made that ε_{ν_1} is approximately equal to ε_{ν_2} such that

$$\frac{I_{\nu_1} - I_{\nu_1}^{clr}}{I_{\nu_2} - I_{\nu_2}^{clr}} = \frac{\int_{p_s}^{p_c} T_{\nu_1}(p, 0) \frac{\partial B_{\nu_1}(p)}{\partial p} dp}{\int_{p_s}^{p_c} T_{\nu_2}(p, 0) \frac{\partial B_{\nu_2}(p)}{\partial p} dp}$$

Because CO₂ is stable within the atmosphere, the transmittance profiles for the two spectral bands can be pre-calculated. Moreover, the temperature profile can be from other sources and the clear-sky radiance can be calculated using RTM or inferred from analyses of satellite clear radiance observations. A set of LUTs can then be calculated, allowing for the inference of cloud-top pressure (height) from the two LW bands.

Due to the nature of the weighting functions in the 15 μm CO₂ band, CO₂ slicing is most effective for the analysis of mid- to high-level clouds, especially semi-transparent clouds such as cirrus.

Cloud top height retrieval

17

4 ALGORITHM DESCRIPTION

4.1 Algorithm Overview

The ACHA serves a critical role in the GOES-R ABI processing system. It provides a fundamental cloud property but also provides information needed by other cloud and non-cloud algorithms. As such, latency was a large concern in developing the ACHA. The current version of the ACHA algorithm draws on the following heritage algorithms:

- The CLAVR-x split-window cloud height from NESDIS, and
- The MODIS CO₂ cloud height algorithm developed by the UW/CIMSS.
- The GOES-R AWG 11/12/13.3 μm algorithm.

The ACHA derives the following cloud products (* = delivered as a cloud CDR to NCDC):

- Cloud-top temperature*,
- Cloud-top pressure*,
- Cloud-top height*, and
- Quality flags*,
- Cloud 11 μm emissivity,
- Cloud microphysical index (β),
- Cloud optical depth,
- Cloud particle size
- Lower cloud level temperature under overlapping condition
- Ice cloud fraction
- Cloud Type (modified by ACHA)

Section 3.4 describes the full set of outputs from the ACHA algorithm.

4.2 Processing Outline

The processing outline of the ACHA is summarized in Figure 1. The current ACHA is implemented with the NOAA/NESDIS/STAR GOES-R AIT processing framework (FRAMEWORK). FRAMEWORK routines are used to provide all of the observations and ancillary data to the algorithms. The ACHA is designed to run on segments of data where a segment consists of multiple scan lines.

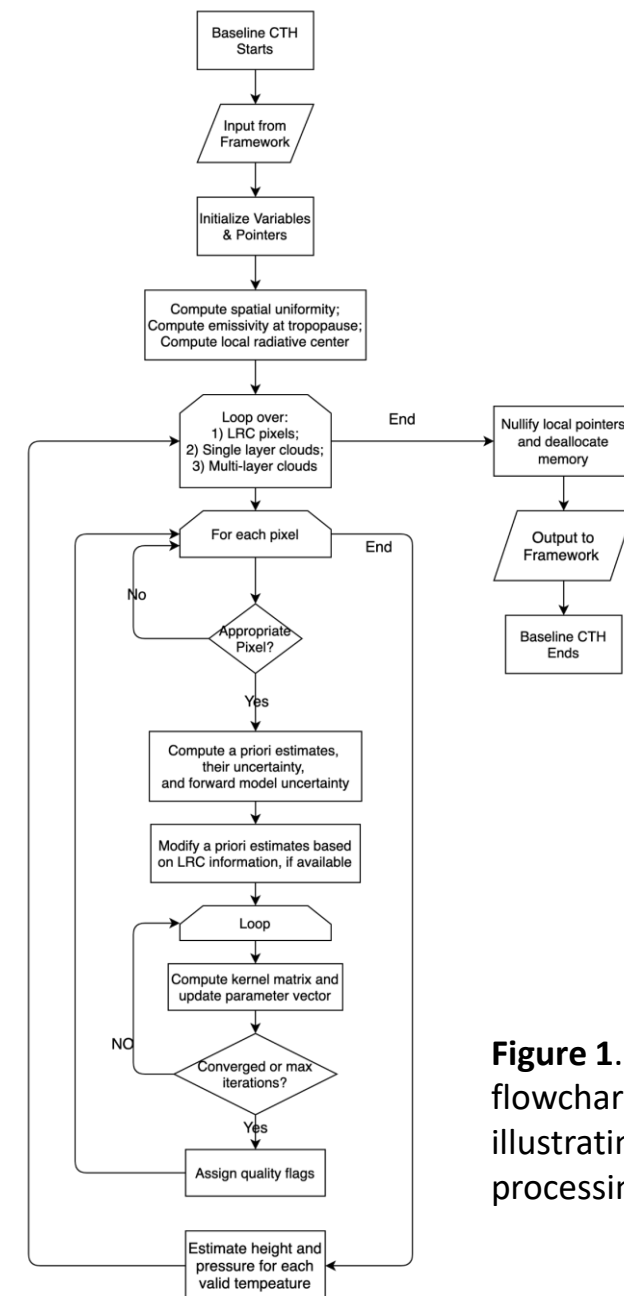
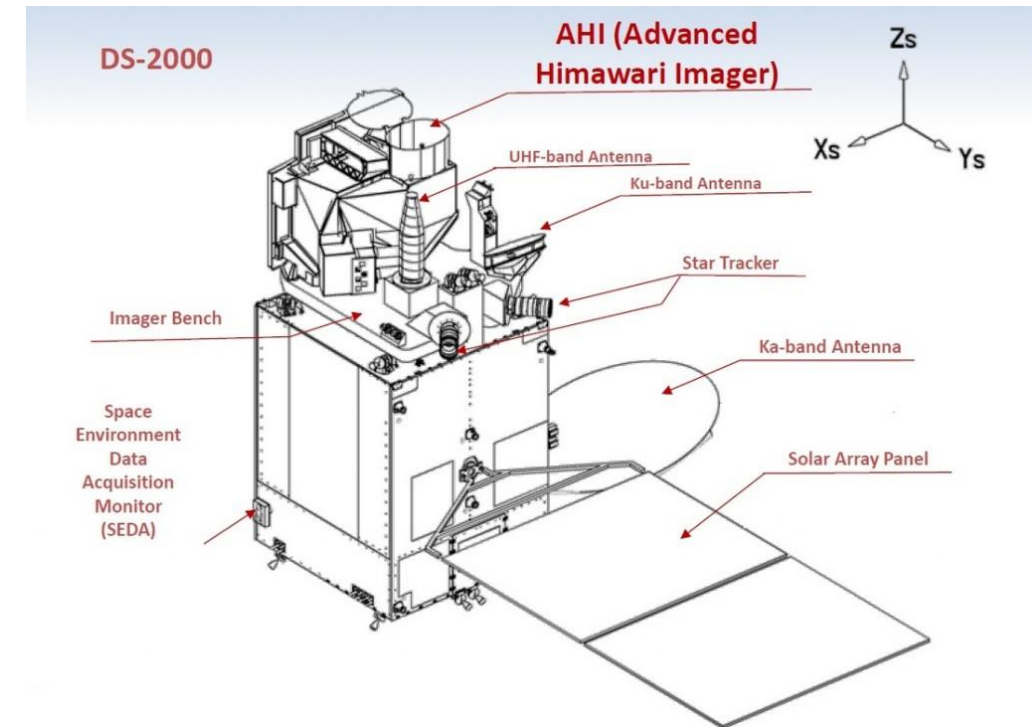
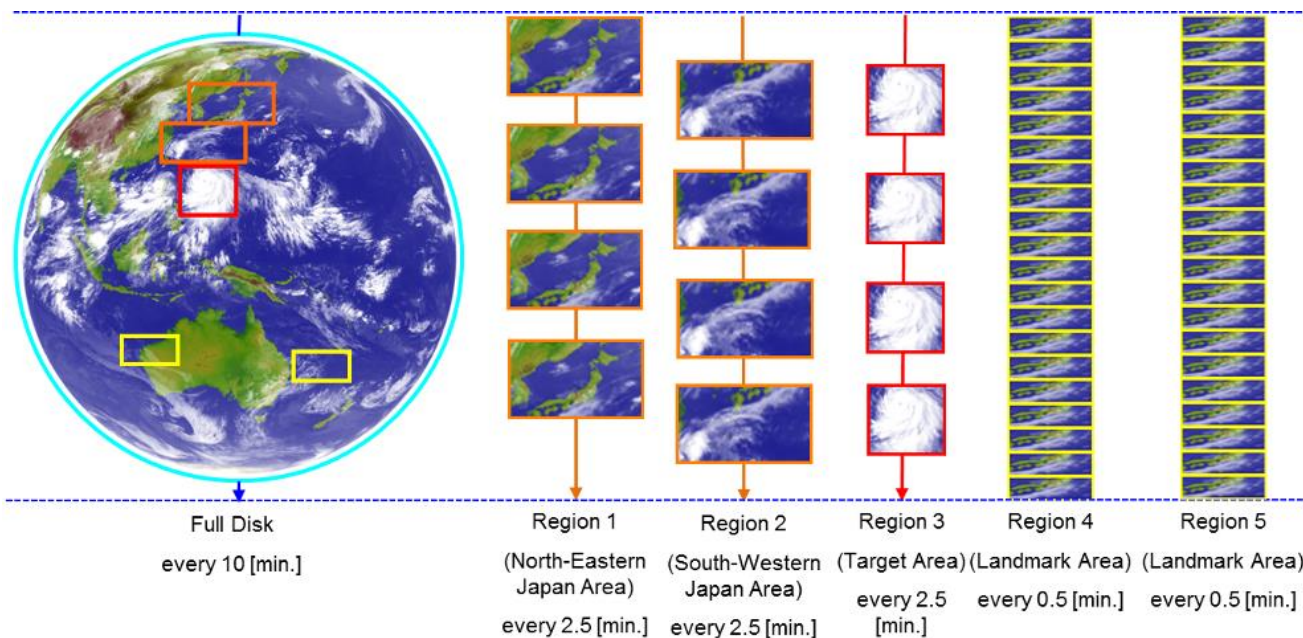


Figure 1. High level flowchart of the ACHA illustrating the main processing sections.

Moderate resolution optical imager

- Example instrument: AHI
- Example product: CTH

- Instrument: **AHI** (Advanced Himawari Imager)
- Website: https://www.data.jma.go.jp/mscweb/en/himawari89/space_segment/spsg_ahi.html
- Data: <https://registry.opendata.aws/noaa-himawari/>

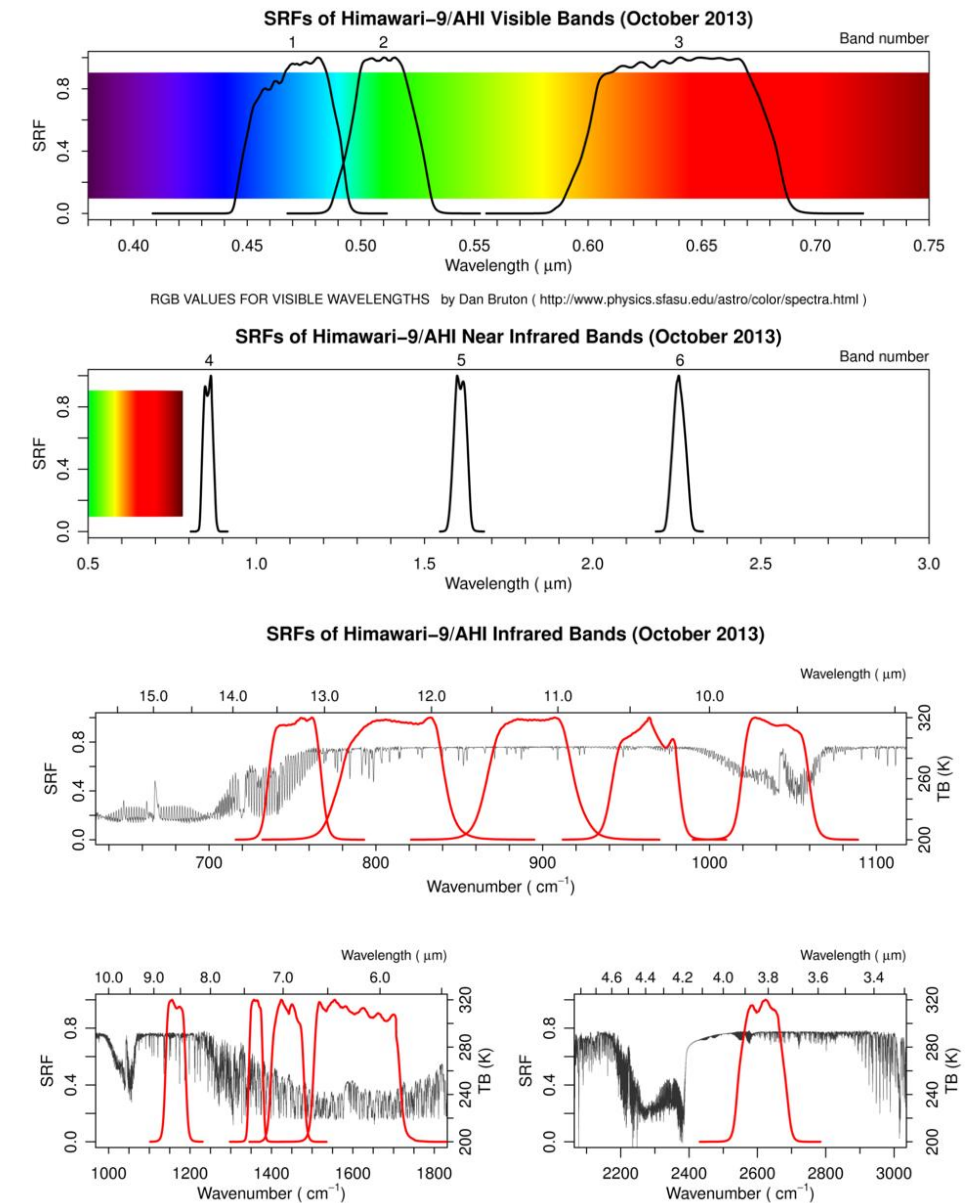


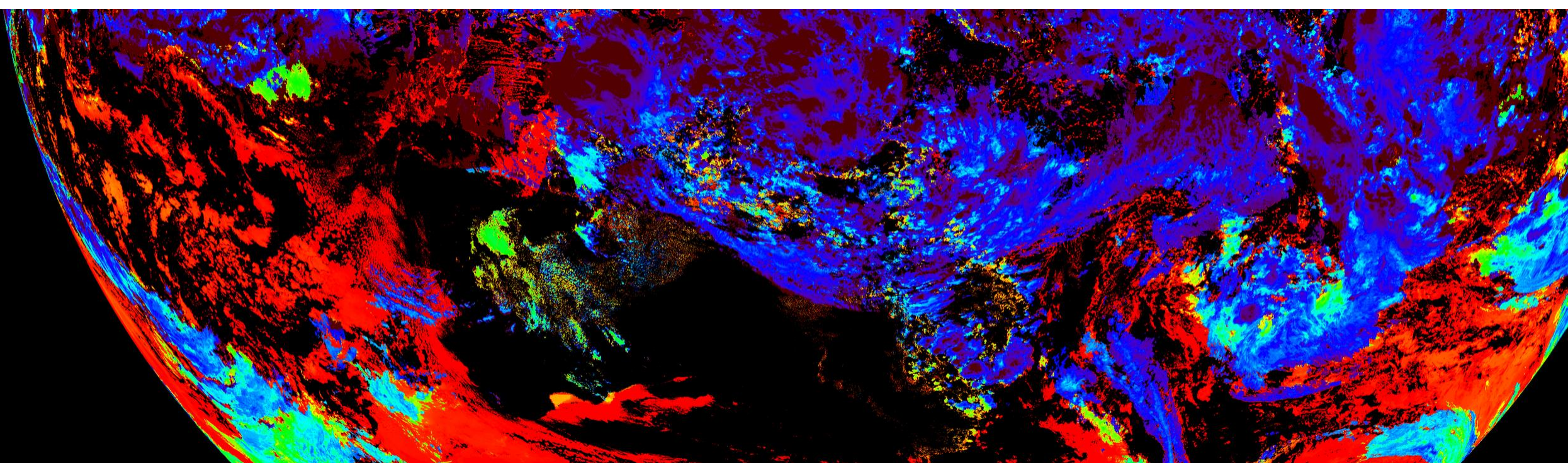
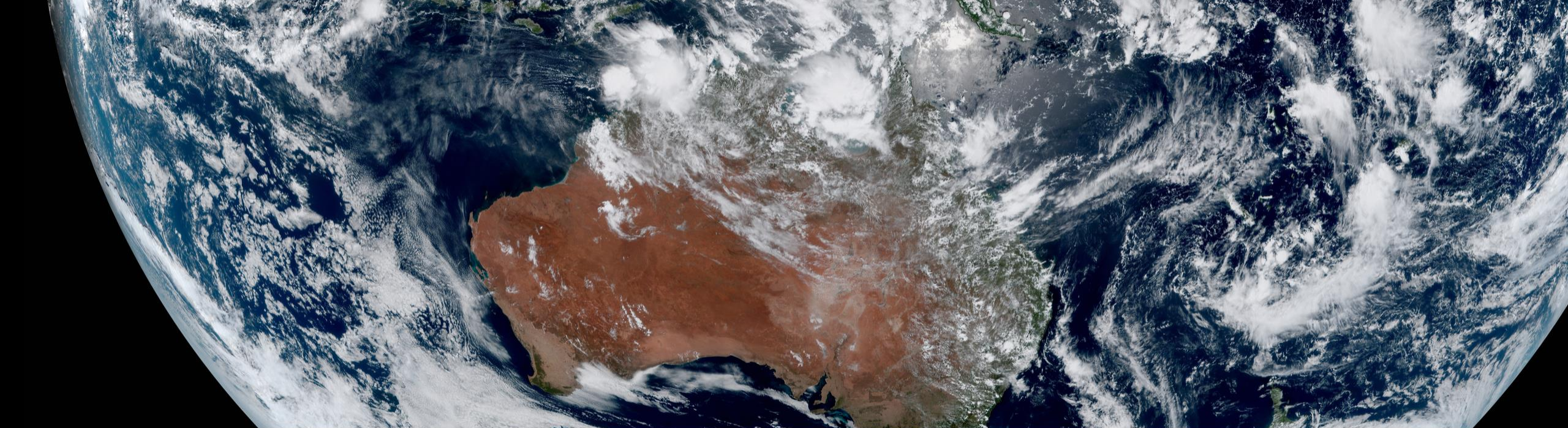
- Short description: 16 channels, balanced VIS, NIR, SWIR, MWIR and TIR.
- Resolution: From 0.5 km to 2 km, depending on spectral band.
- Coverage / Cycle: Full disk in 10 min. Limited areas in proportionally shorter intervals.

AHI instrument specification

Wave length [μm]	Himawari-8/9				MTSAT-1R/2	
	Band number	Spatial resolution at SSP [km]	Central wave length [μm]		Channel name	Spatial resolution at SSP [km]
			AHI-8 (Himawari-8)	AHI-9 (Himawari-9)		
0.47	1	1	0.47063	0.47059	-	-
0.51	2	1	0.51000	0.50993	-	-
0.64	3	0.5	0.63914	0.63972	VIS	1
0.86	4	1	0.85670	0.85668	-	-
1.6	5	2	1.6101	1.6065	-	-
2.3	6	2	2.2568	2.2570	-	-
3.9	7	2	3.8853	3.8289	IR4	4
6.2	8	2	6.2429	6.2479	IR3	4
6.9	9	2	6.9410	6.9555	-	-
7.3	10	2	7.3467	7.3437	-	-
8.6	11	2	8.5926	8.5936	-	-
9.6	12	2	9.6372	9.6274	-	-
10.4	13	2	10.4073	10.4074	IR1	4
11.2	14	2	11.2395	11.2080	-	-
12.4	15	2	12.3806	12.3648	IR2	4
13.3	16	2	13.2807	13.3107	-	-

SSP: sub satellite point





Air temperature profile retrieval

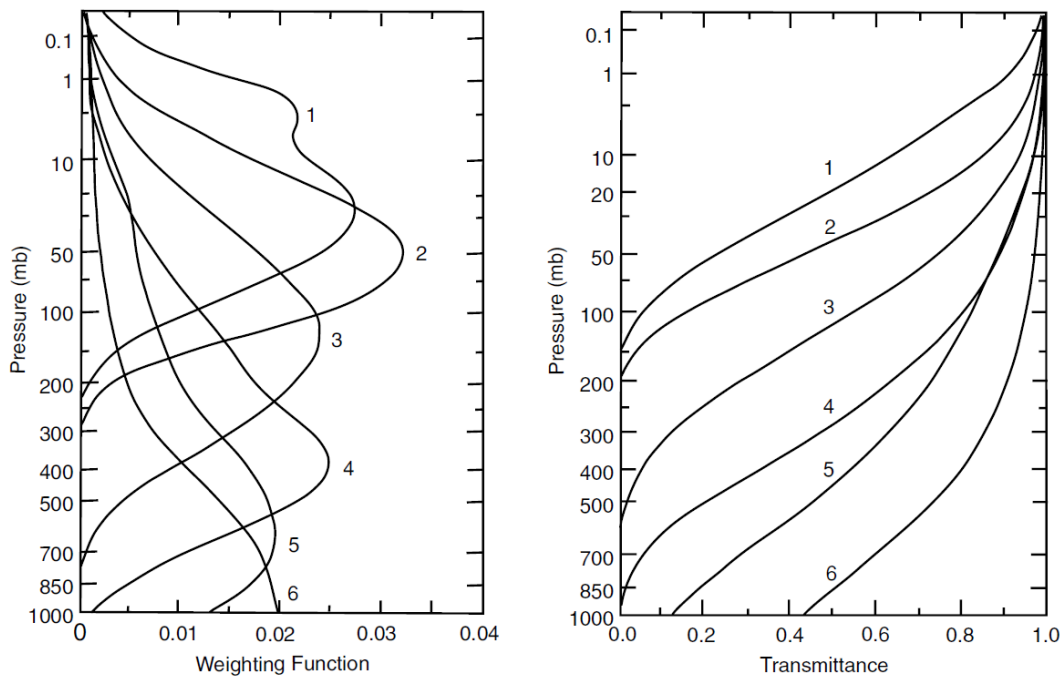


Figure 7.15 The weighting function and transmittance for the NOAA 2 Vertical Temperature Profile Radiometer (VTPR).

*VTPR consists of 6 bands at around 15 um CO₂ absorption band. The central wavelengths of these bands are 14.95 um, 14.77 um, 14.38 um, 14.12 um, 13.79 um, and 13.38 um.

From CTH retrieval, for clear-sky, we have

$$I_v^{clr} = B_v(T_s)T_v(p_s, 0) + \int_{p_s}^0 B_v(p) \frac{\partial T_v(p, 0)}{\partial p} dp$$

For bands at around 15 um CO₂ absorption line, we can see that $T_v(p_s, 0) = 0$. Thus, we can drop $B_v(T_s)T_v(p_s, 0)$ from these bands,

$$I_v^{clr} = \int_{p_s}^0 B_v(p) \frac{\partial T_v(p, 0)}{\partial p} dp$$

Since the Planck function is smooth and in a small spectral interval, it can be approximated in a linear form as $B_v(T) = c_v B_{v_r}(T) + d_v$ where v_r is the reference wavenumber, c_v and d_v are fitting coefficients.

The above equation can then be rewritten as,

$$g_v = \int_{p_s}^0 f(p) K_v(p) dp$$

where we let

$$g_v = \frac{I_v - d_v}{c_v}, \quad f(p) = B_{v_r}[T(p)], \quad K_v(p) = \frac{\partial T_v(p, 0)}{\partial p}$$

$K_v(p)$ is the weighting function; and the $f(p)$ is the function to be resolved from a set of g_v .

Air temperature profile retrieval



Animation of AIRS Collects Data and Creates a Temperature Profile

Source: NASA/JPL AIRS Project

- Atmospheric temperature profile retrieval from satellite IR observations was first suggested by *King (1956)*.
- *Kaplan (1959)* advanced the sounding concept by demonstrating that vertical resolution of the temperature field can be inferred from the spectral distribution of atmospheric emission. He pointed out that observations in the wings of a spectral band sense deeper into the atmosphere, whereas observations in the band centre see only the very top layer of the atmosphere since the radiation mean free path is small.
- Thus, by properly selecting a set of different sounding wavenumbers, the observed radiances can be used to make an interpretation leading to the vertical temperature distribution in the atmosphere.
- To determine atmospheric temperatures from measurements of thermal emission, the source of emission must be a relatively abundant gas of known and uniform distribution. Otherwise, its uncertainty will make the determination of temperature from the measurements ambiguous.
- In practice, the CO_2 absorption line at $15 \mu\text{m}$ is used for retrieving air temperature profile.

Cross-nadir infrared sounder

- Example instrument: AIRS
- Example product: Temperature profile

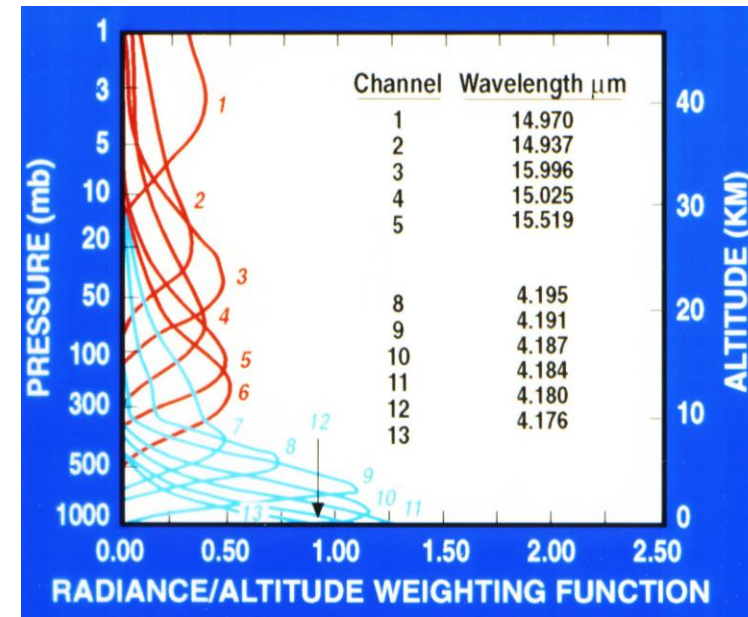
Instrument: **AIRS** (Atmospheric InfraRed Sounder)

Website: <https://airs.jpl.nasa.gov/>

Data: <https://airsl1.gesdisc.eosdis.nasa.gov/data/>

- The main purpose for AIRS is temperature/humidity sounding, ozone profile and total-column green-house gases.
- The AIRS instrument suite consists of the hyperspectral AIRS instrument with 2378 infrared channels and 4 visible/near-infrared channels. It was often used with the microwave radiometer (AMSU-A) onboard the same satellite, EOS-Aqua.
- AIRS infrared technology creates three-dimensional maps of air and surface temperature, water vapor, and cloud properties.
- It was suggested by the Joint Center for Satellite Data Assimilation that significant improvement in forecast skill has been achieved with the assimilation of AIRS data.

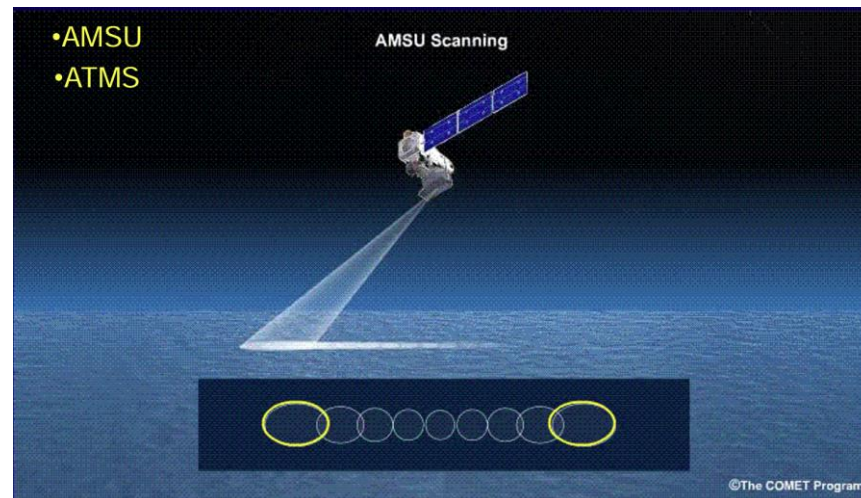
Spectral range (μm)	Spectral range (cm^{-1})	Spectral resolution	Spatial resolution
3.74 - 4.61 μm	2170 - 2674 cm^{-1}	$\sim 2.0 \text{ cm}^{-1}$	13.5 km
6.20 - 8.22 μm	1216 - 1613 cm^{-1}	$\sim 1.0 \text{ cm}^{-1}$	13.5 km
8.80 - 15.4 μm	650 - 1136 cm^{-1}	$\sim 0.5 \text{ cm}^{-1}$	13.5 km
0.41 - 0.44 μm	not relevant	30 nm	2.3 km
0.58 - 0.68 μm	not relevant	100 nm	2.3 km
0.71 - 0.92 μm	not relevant	210 nm	2.3 km
0.49 - 0.94 μm	not relevant	N/A (broadband)	2.3 km



High spectral resolution sampling of CO₂ signature provides 1 km height resolution.

Passive microwave radiometer

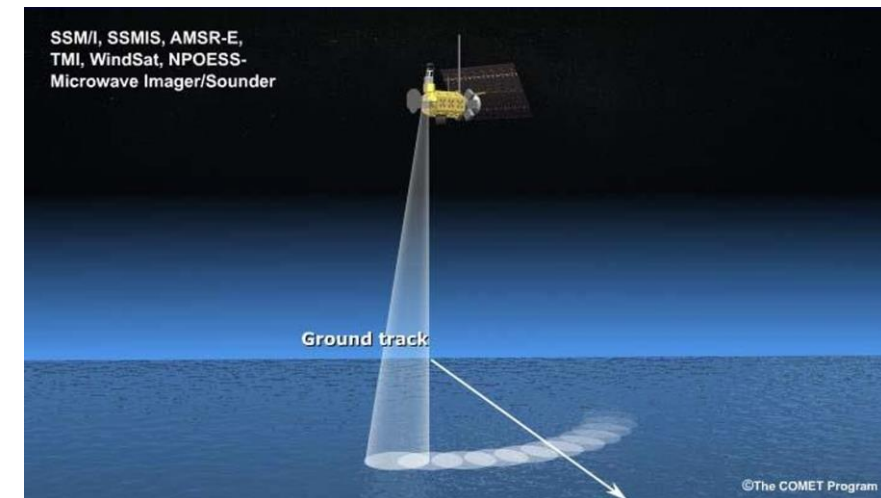
Cross-track scan



Advantage: Larger coverage swath relative to conical scan.

Disadvantage: Resolution varies across the swath (degraded spatial resolution as the viewing angle increases relative to nadir)

Conical scan



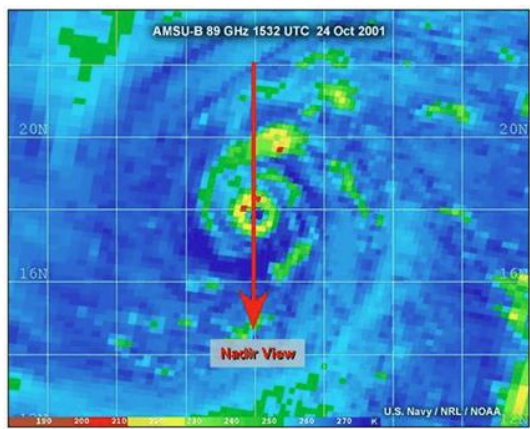
Advantage: Resolution remains constant because scan footprints are the same size throughout the entire swath.

Disadvantage: Narrower coverage swath relative to cross-track scan.

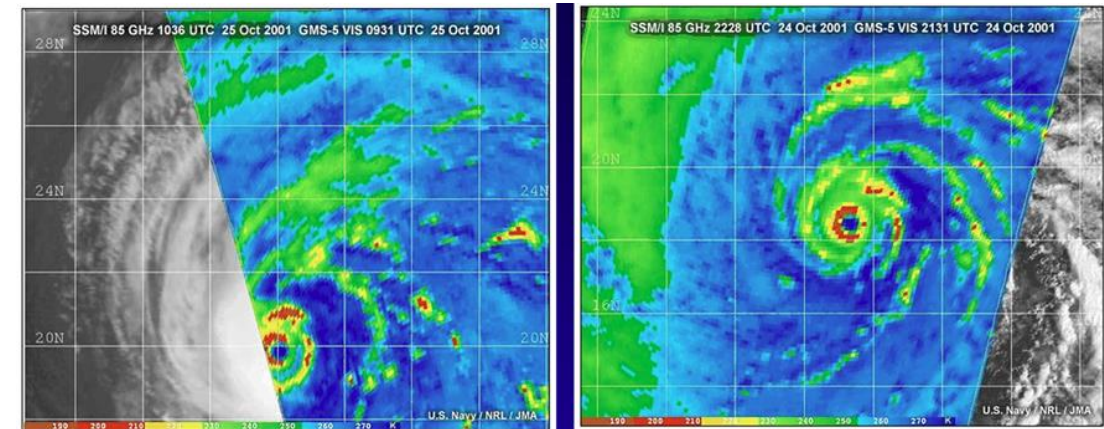
Images courtesy COMET

Passive microwave radiometer

Cross-track scan



Conical scan



Advantage: Larger coverage swath relative to conical scan.

Disadvantage: Resolution varies across the swath (degraded spatial resolution as the viewing angle increases relative to nadir)

Advantage: Resolution remains constant because scan footprints are the same size throughout the entire swath.

Disadvantage: Narrower coverage swath relative to cross-track scan.

Passive microwave radiometer

- Below 40 GHz only the weakly absorbing pressure-broadened 22.235 GHz water vapor line is dominant.
- O_2 has a strong band of magnetic dipole transitions near 60 GHz and a single transition at 118.75 GHz.
- At 183 GHz, water vapor absorption again becomes dominant because of the strongly absorbing line.

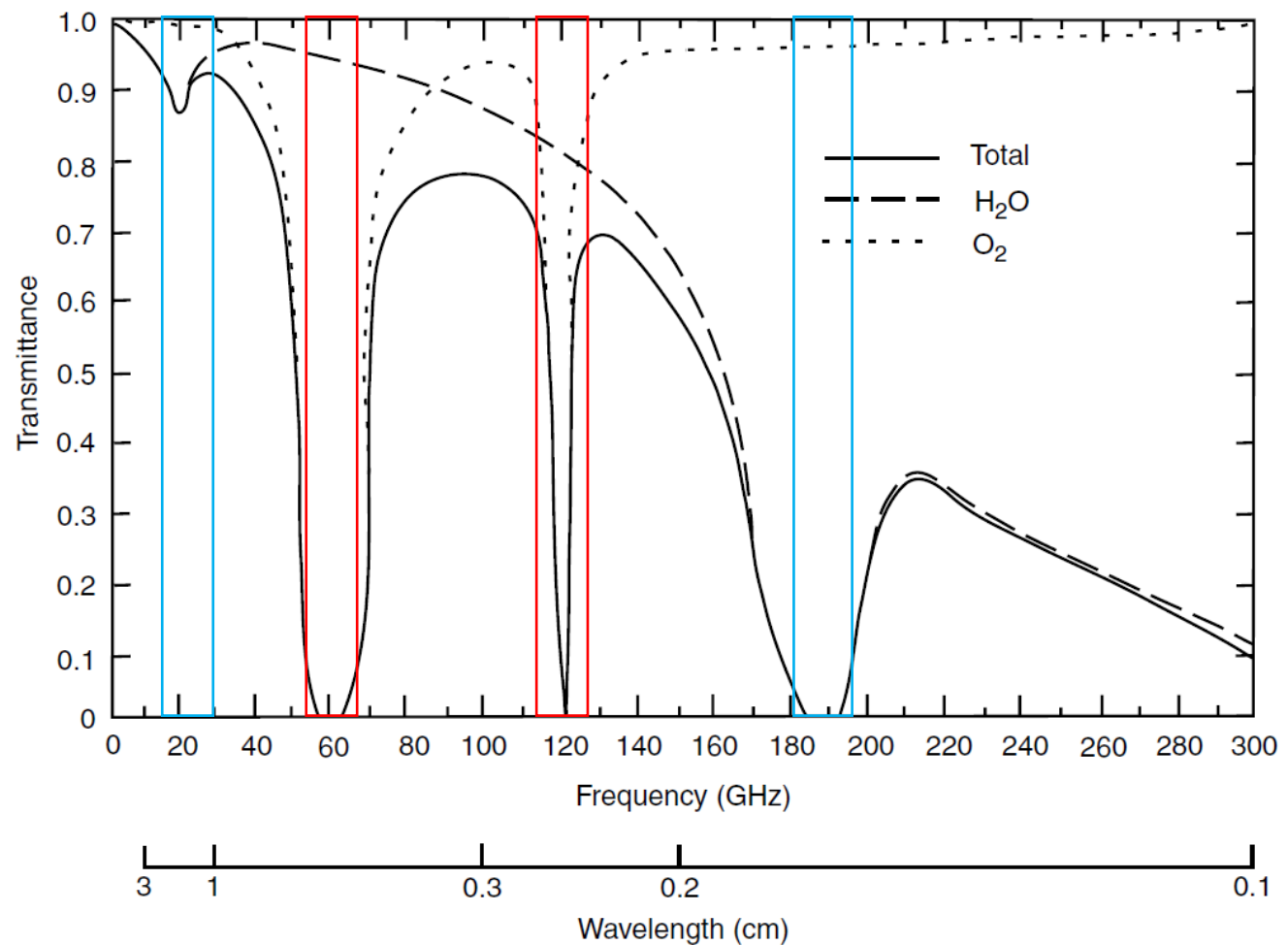
- Considering the size of water droplets ($\sim 10 \mu\text{m}$) and ice crystals ($\sim 100 \mu\text{m}$) in the atmosphere, their effects on the scattering of microwaves ($\sim 1 \text{ cm}$) are generally small.
- RTE for a nonscattering atmosphere in local thermodynamic equilibrium is given by,

$$I_{\tilde{\nu}}(0) = I_{\tilde{\nu}}(p_s)T_{\tilde{\nu}}(p_s, 0) + \int_{p_s}^0 B_{\tilde{\nu}}[T(p)] \frac{\partial T_{\tilde{\nu}}(p, 0)}{\partial p} dp$$

where

$$I_{\tilde{\nu}}(p_s) = \varepsilon_{\tilde{\nu}}B(T_s) + (1 - \varepsilon_{\tilde{\nu}}) \int_0^{p_s} B_{\tilde{\nu}}[T(p)] \frac{\partial T_{\tilde{\nu}}(p_s, p)}{\partial p} dp$$

→ $I_{\tilde{\nu}}(0) = \varepsilon_{\tilde{\nu}}B(T_s)T_{\tilde{\nu}}(p_s, 0) + (1 - \varepsilon_{\tilde{\nu}})T_{\tilde{\nu}}(p_s, 0) \int_0^{p_s} B_{\tilde{\nu}}[T(p)] \frac{\partial T_{\tilde{\nu}}(p_s, p)}{\partial p} dp + \int_{p_s}^0 B_{\tilde{\nu}}[T(p)] \frac{\partial T_{\tilde{\nu}}(p, 0)}{\partial p} dp$



Demonstrative atmospheric transmittances (total, H_2O , O_2) as a function of frequency and wavelength in the MW region.

Passive microwave radiometer

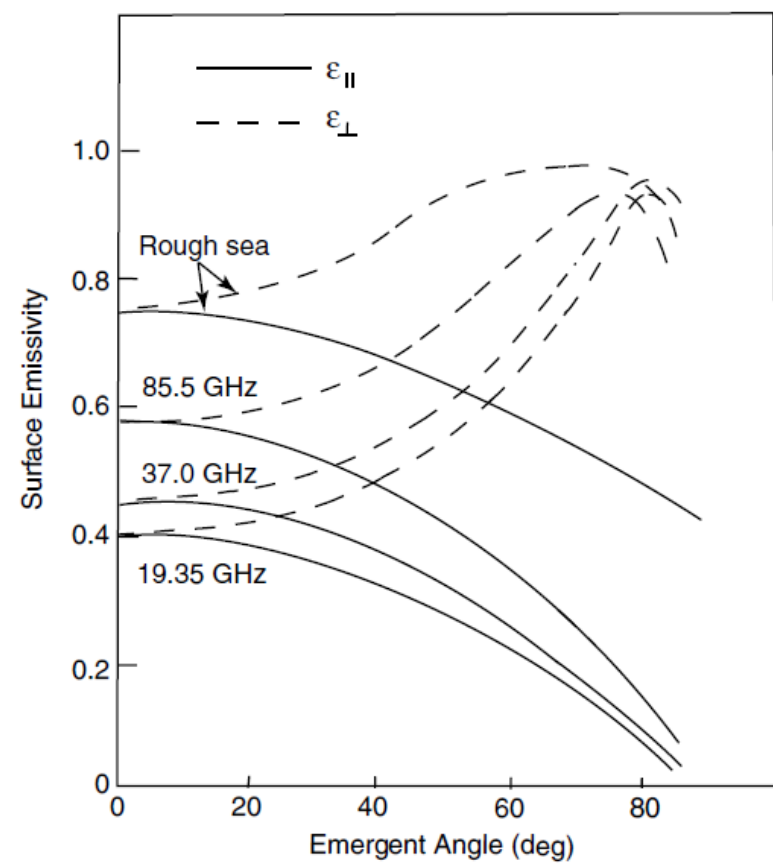


Figure 7.25 Emissivities of calm and rough ocean surfaces for a number of microwave frequencies. The solid and dashed curves represent the horizontal ε_{\parallel} and vertical ε_{\perp} polarization components, respectively (data taken from Huang and Liou, 1983).

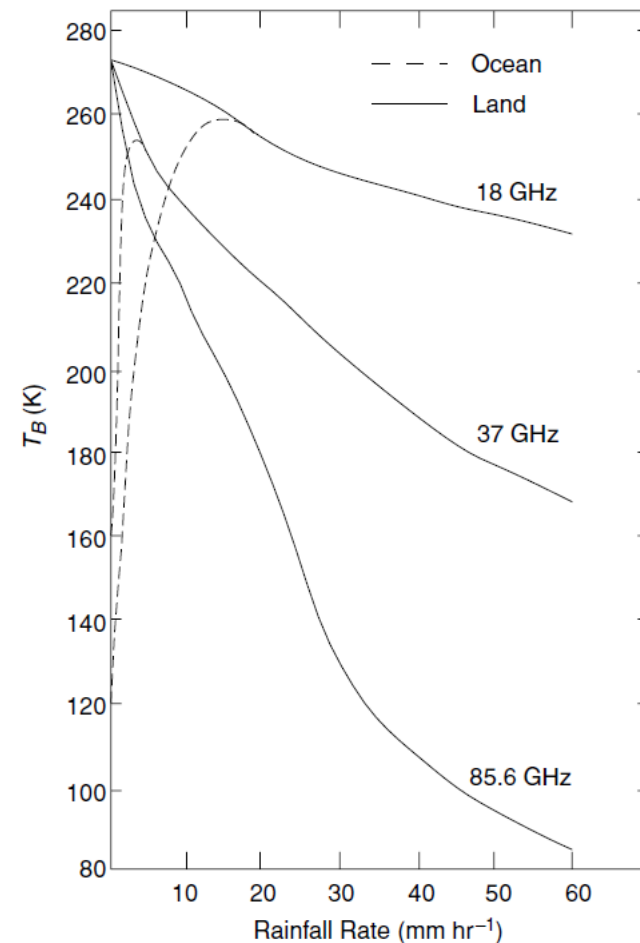


Figure 7.26 Brightness temperature as a function of rainfall rate over the ocean and land for three frequencies (data taken from Spencer *et al.*, 1989).

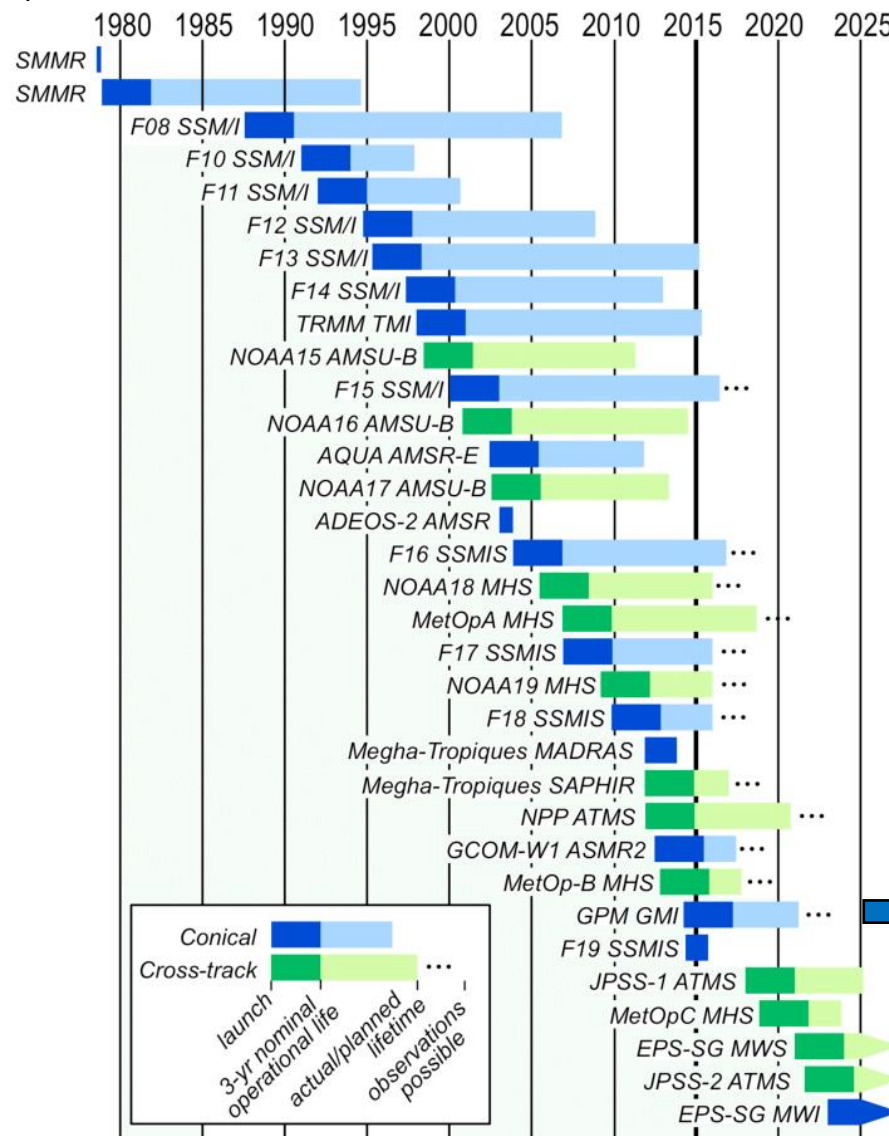
Cross-track microwave radiometer

- Example instrument: GMI
- Example product: Precipitation

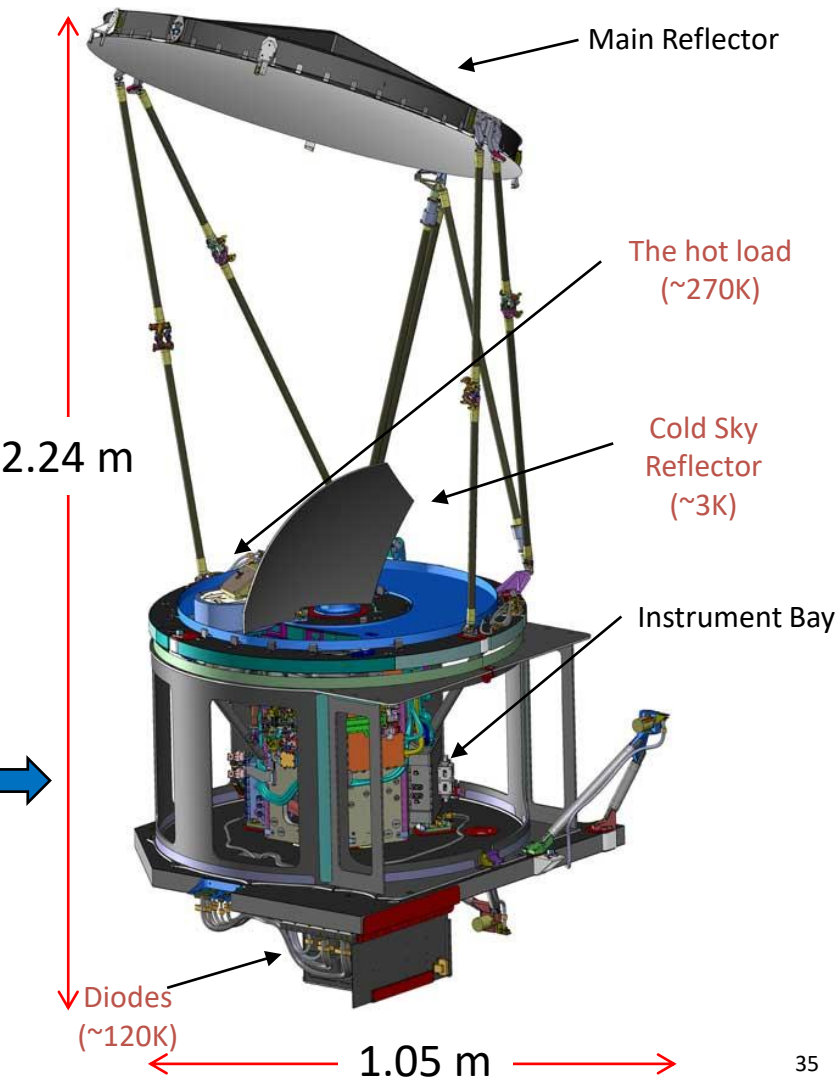
Some MW sensors...

- SMMR (Scanning Multichannel Microwave Radiometer): 5-frequency, 10-channel between 6.6-37 GHz.
- SSM/I (Special Sensor Microwave – Imager): 4 frequencies, 7-channels between 19.35-85 GHz.
- TMI (TRMM Microwave Imager): 5 frequencies, 9 channels between 10.65-85.5 GHz.
- AMSU-B (Advanced Microwave Sounding Unit – B): 5 channels including the 183 GHz band.
- MHS (Microwave Humidity Sounding): 5 channels including the 183 GHz band.
- SSMS (Special Sensor Microwave - Imager/Sounder): 21 frequencies, 24 channels MW radiometer covering the 54 and 183 GHz bands.
- ATMS (Advanced Technology Microwave Sounder): 22 channels including the 54 and 183 GHz bands.
- GMI (GPM Microwave Imager): 8 frequencies, 13 channels

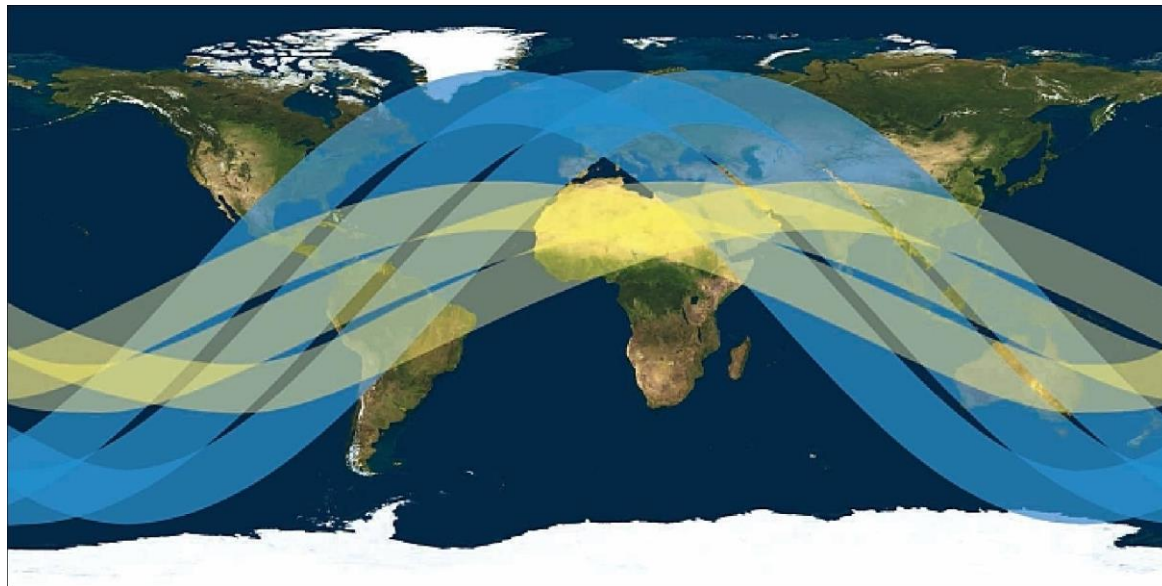
Time history of passive microwave sensors



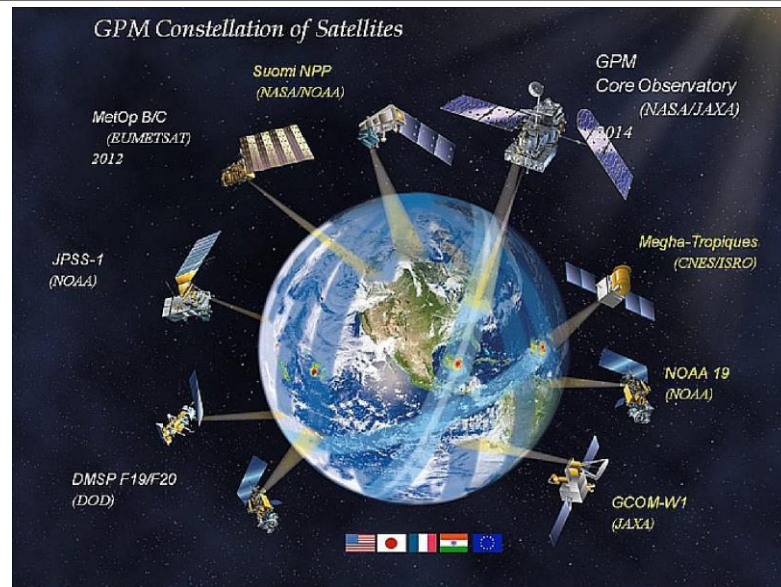
GMI self-calibrates to an absolute accuracy of 5K!



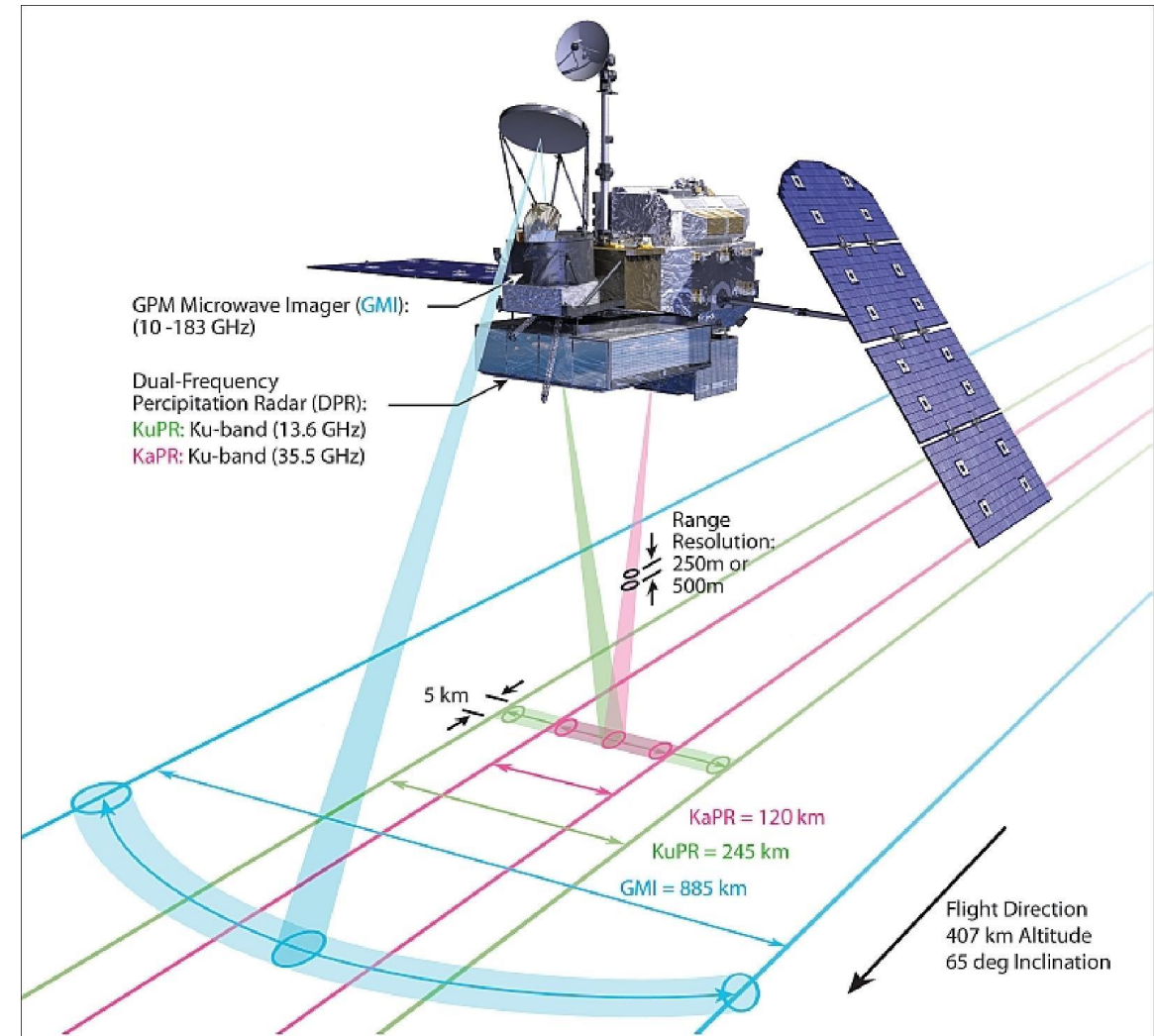
Global Precipitation Measurement (GPM)



Orbits of GPM (blue) and TRMM (yellow)
(image credit: NASA)

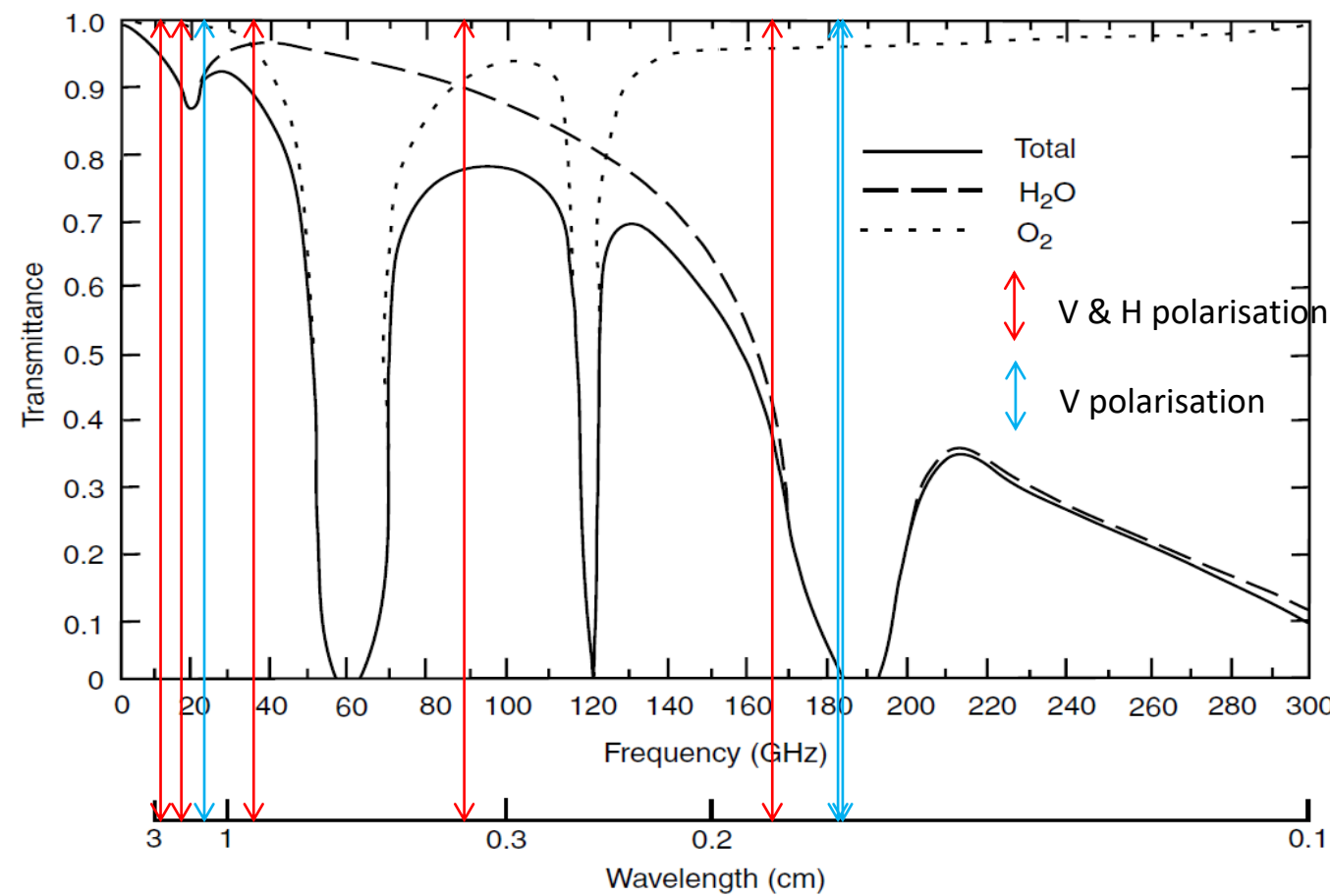


GPM mission architecture
(image credit: NASA)



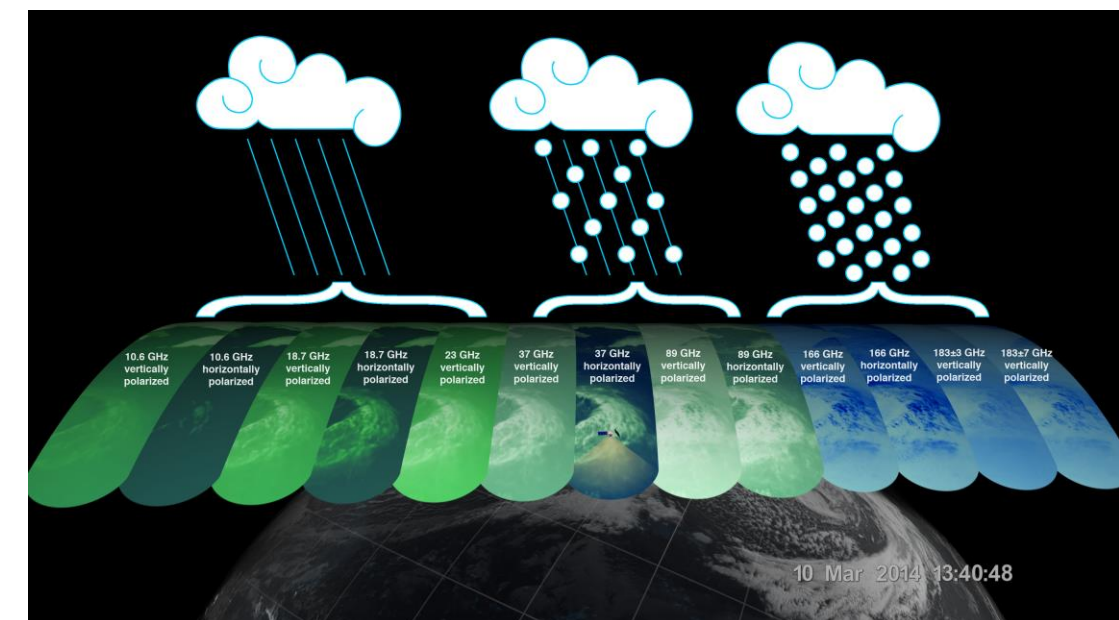
Schematic view of the observation geometries with the GPM CORE instruments (image credit: NASA)

GPM Microwave Imager (GMI)



GMI performance characteristics

Frequency (GHz)	Polarization	NEDT/Reqmt (K)	Expected* NEDT	Expected Beam Efficiency (%)	Expected Calibration Uncert.	Resolution (km)
10.65	V/H	0.96	0.96	91.4	1.04	26
18.7	V/H	0.84	0.82	92.0	1.08	15
23.8	V	1.05	0.82	92.5	1.26	12
36.5	V/H	0.65	0.56	96.6	1.20	11
89.0	V/H	0.57	0.40	95.6	1.19	6
165.5	V/H	1.5	0.81	91.9	1.20	6
183.31±3	V	1.5	0.87	91.7	1.20	6
183.31±7	V	1.5	0.81	91.7	1.20	6



GPM Precipitation Product

1. GPM relies on passive and active measurements to measure the properties of precipitation.
 - GPM's Dual-Frequency Precipitation Radar (DPR) transmit and receive signals reflected back to the radar. The Ku-band (13.6 GHz) is sensitive to moderate rain rates while the Ka-band (35.5 GHz) is sensitive to lighter rain and falling snow.
 - GPM Microwave Imager (GMI) measure natural thermal radiation from the complete observational scene including snow, rain, clouds, and the Earth's surface.
2. The GPM radiometer algorithm is based upon a Bayesian approach in which the GPM core satellite is used to create an a-priori database of observed cloud and precipitation profiles. In this approach, the probability of a particular profile \mathbf{R} , given \mathbf{T}_b can be written as:

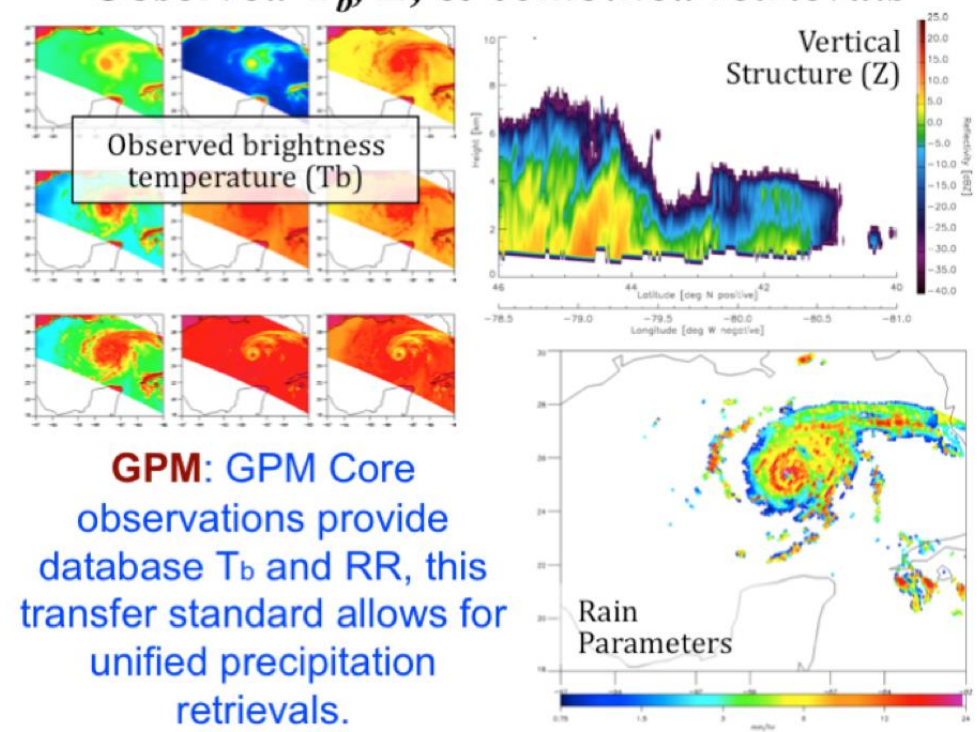
$$\Pr(\mathbf{R}|\mathbf{T}_b) = \Pr(\mathbf{R}) \times \Pr(\mathbf{T}_b|\mathbf{R})$$

$\Pr(\mathbf{R})$ is the probability that a certain profile \mathbf{R} will be observed, which can be derived from the a-priori database of rain profiles established by the radar/radiometer observing systems

$\Pr(\mathbf{T}_b|\mathbf{R})$ is the probability of observing the brightness temperature vector, \mathbf{T}_b , given a particular rain profile \mathbf{R} . It is obtained from radiative transfer computations through the cloud model profiles.

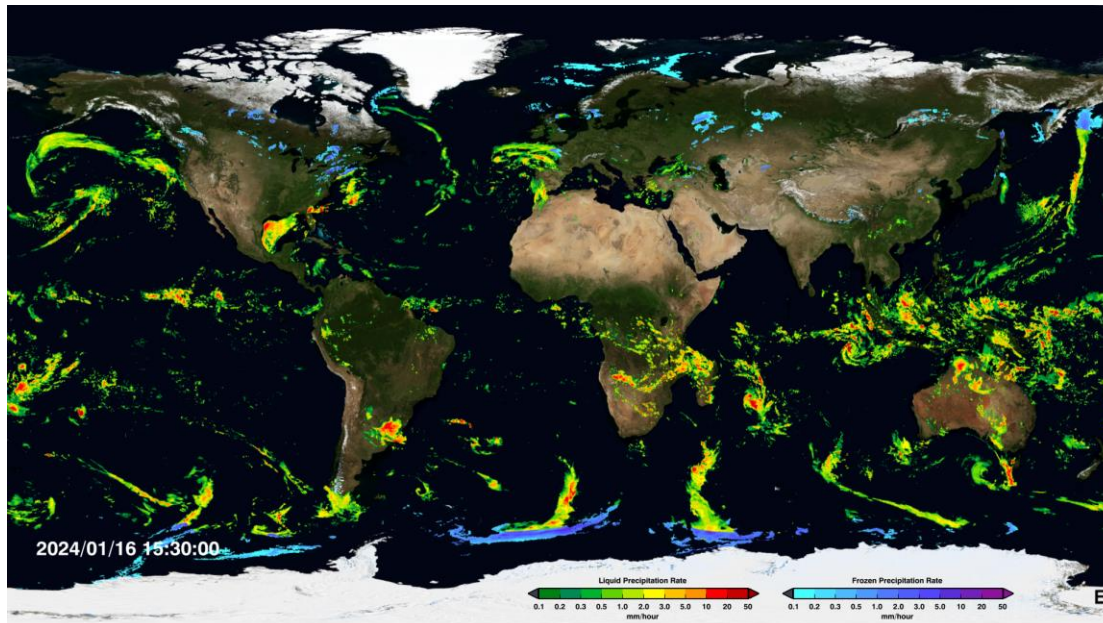
3. The retrieval procedure can be said to compose a new hydrometeor profile by taking the weighted sum of structures in the cloud structure database that are radiometrically consistent with the observations.
4. In using the Bayesian inversion approach, an important step is to select the appropriate *a-priori* profiles. Operationally, the *a-priori* database is subsetted by 2-meter temperature (T2M), TCWV and Land Surface Classification, as well as an airmass lifting index (ALI) for mountain rain only.

**GPM's database from DPR+GMI obs.
Observed T_b , Z, & combined retrievals**



GPM Precipitation Product

NASA's Integrated Multi-satellitE Retrievals for GPM (IMERG) - <https://gpm.nasa.gov/data/imerg>



JAXA's Global Satellite Mapping of Precipitation (GSMaP) - <https://sharaku.eorc.jaxa.jp/GSMaP/>

